Gezeiten sind überall

Die Erde unter dem Einfluss von Mond und Sonne

Walter Zürn

Geophysiker i. R.

Observatorium Schiltach - Black Forest Observatory

Wettzell

Geodätisches Informationszentrum

21. Juni 2007

Übersicht

- Grundlagen
- Gezeiten der Meere und Seen
- Gezeiten der festen Erde
- Spektakuläre Gezeiten im Sonnensystem

- Ich entschuldige mich für häufige Verwendung von englischen Ausdrücken

Newton's Law of Gravitation

$$\mathbf{F} = \mathbf{-}\ \mathbf{G} \cdot \frac{M_1 \cdot M_2}{r^2}$$

G = Gravitational constant = $6.674 \cdot 10^{-11}\ m^3 kg^{-1} s^{-2}$

Tidal forces ≙ differences in gravitational forces which arise in an <u>extended body</u> in an <u>inhomogeneous gravity field</u>

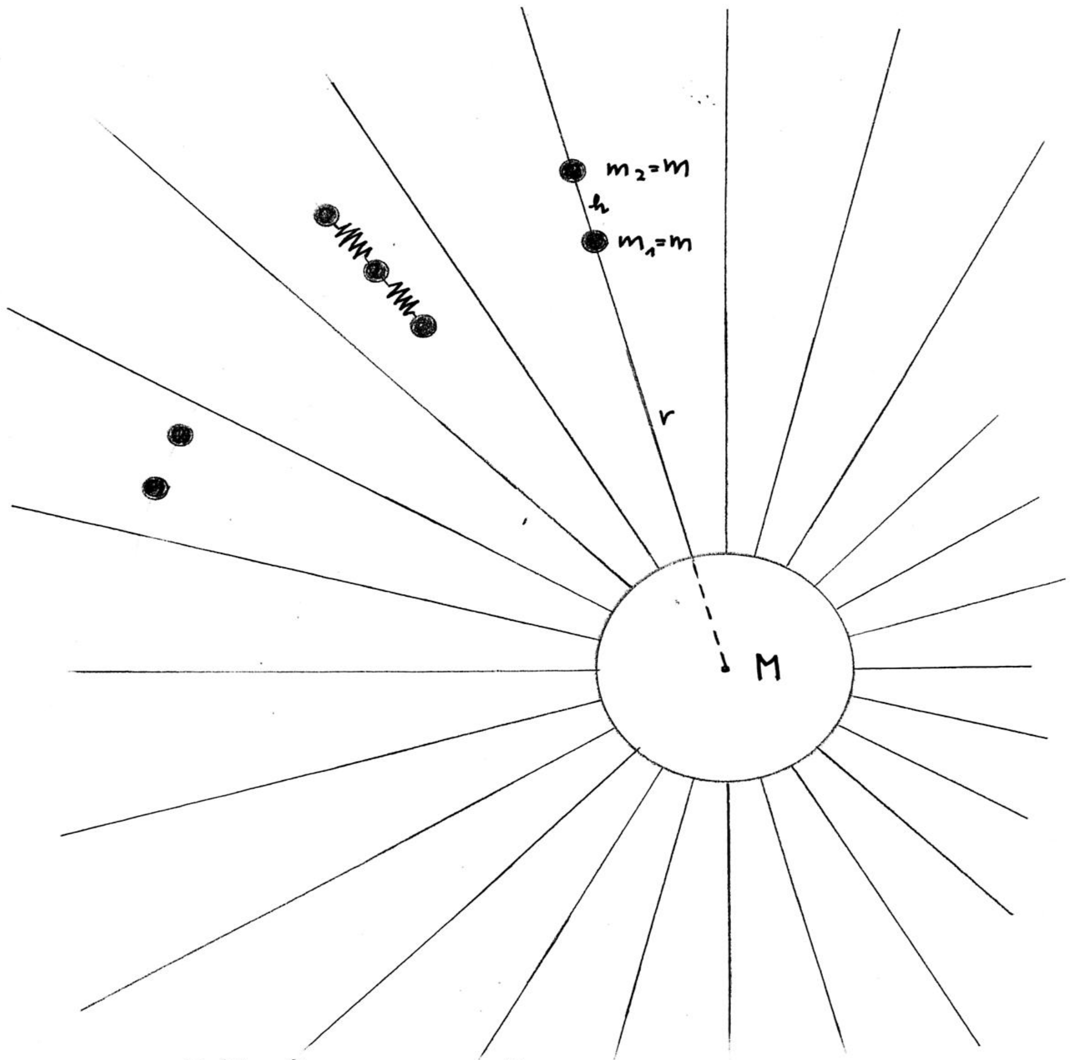

$$\Delta K_{12} \doteq -\frac{G \cdot Mm}{r^2}\left[1 - \frac{1}{\left(1+\frac{h}{r}\right)^2}\right] = -\frac{GMm}{r^3} \cdot h$$

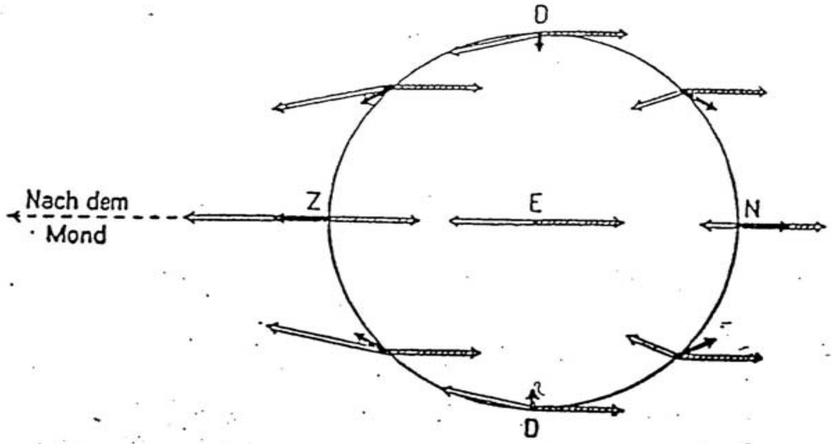
D
Nach dem
Mond
Z
E
N
D

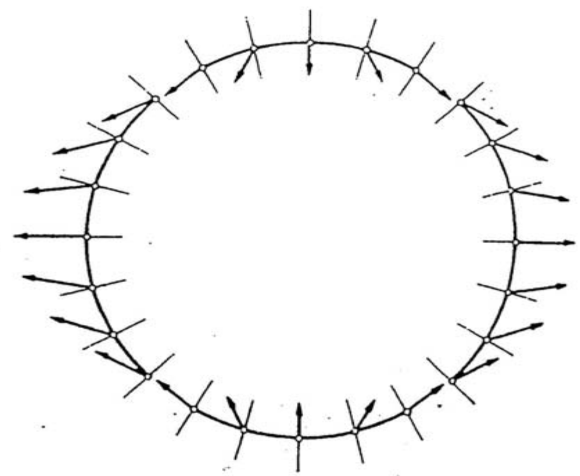

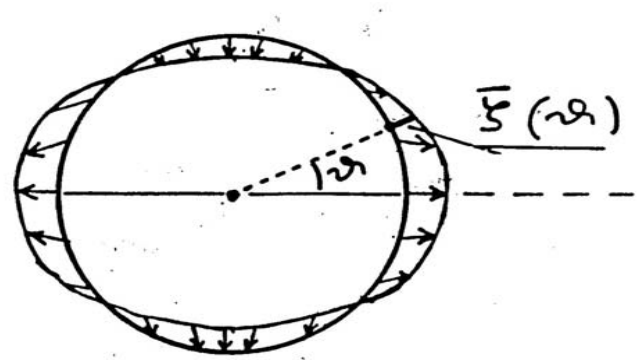
$\bar{\zeta}(\vartheta)$
ϑ

Ecliptic Plane from North Celestial Pole

τ = 1 d
s = ∡ (☾ - ♈) → 27.32 d
h = ∡ (☉ - ♈) → 365.24 d
p = ∡ (Perigee - ♈) → 8.85
N = ∡ (☊ - ♈) → 18.61
p_s = ∡ (Perihelion - ♈) → 20 94
Precession : 26 000 a

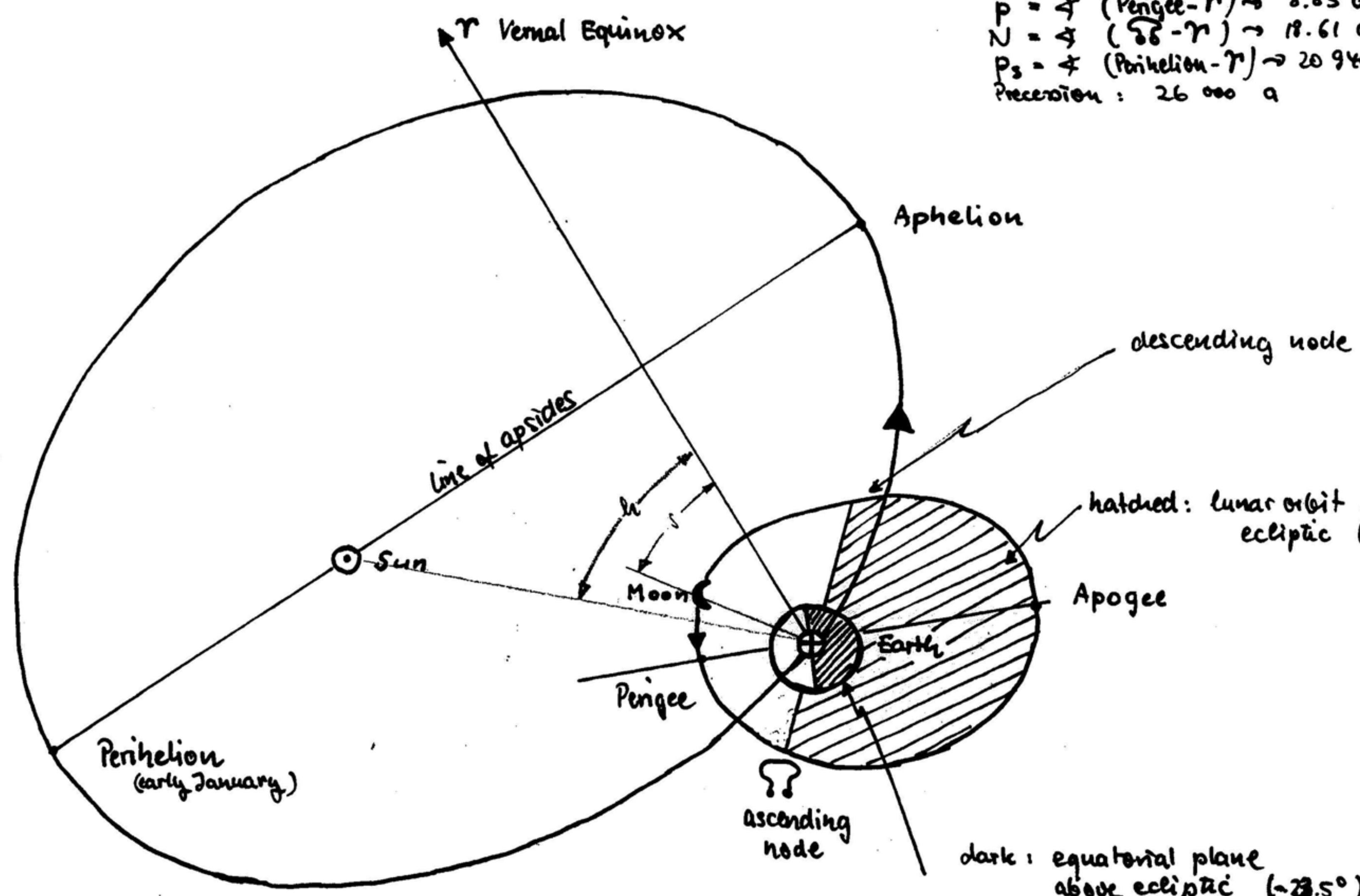

(MELCHIOR)

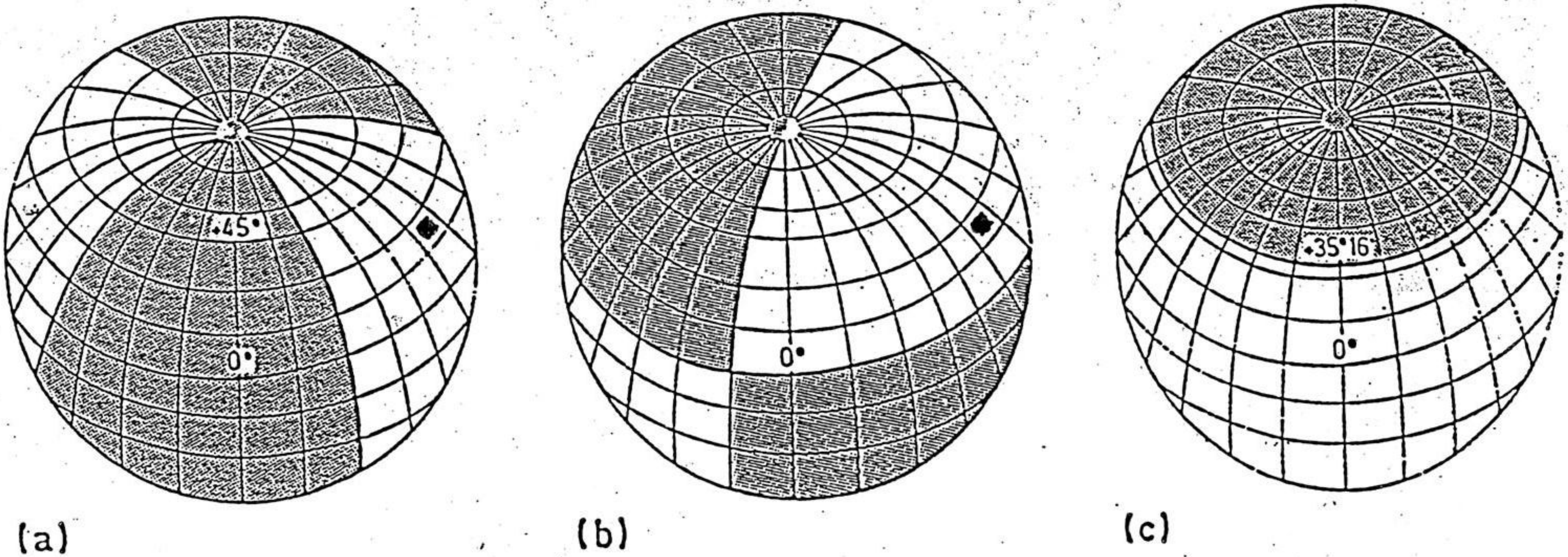

Fig. 1.2. The three kinds of tides

sectorial
semi diurnal

tesseral
diurnal

zonal
long period

Doodson's Constant

$$\mathbf{G}_D(M > E) = \frac{3}{4} \cdot G \cdot \frac{M_M \cdot R_E^2}{r_M^3}$$

$$\mathbf{G}_D(S > E) = \frac{\rho_S}{\rho_M} \cdot \left(\frac{R_S/r_S}{R_M/r_M}\right)^3 \cdot G_D(M > E)$$

$$\mathbf{G}_D(S > E) = 0.46 \cdot G_D(M > E)$$

Vergleich von Gezeitenkräften im Sonnensystem

Mond	>	Erde	1.0
Sonne	>	Erde	0.46
Venus	>	Erde	0.00004
Jupiter	>	Erde	0.0000048
Mars	>	Erde	0.00000086
Merkur	>	Erde	0.00000027
Saturn	>	Erde	0.00000017
Uranus	>	Erde	0.0000000027
Neptun	>	Erde	0.00000000077
Pluto	>	Erde	0.00000000000056
Erde	>	Mond	6.03
Sonne	>	Mond	0.041
Jupiter	>	Io	1450
Jupiter	>	Europa	291

Wichtigste Konstituenten

Bezeichnung		Periode	Amplitude
		Sonnenstunden	M2 = 100.0
Halbtägige Tiden :			
Hauptmondtide	M2	12.42	100.0
Hauptsonnentide	S2	12.00	46.6
Elliptische Mondtide	N2	12.66	19.1
Luni-solare Halbtagstide	K2	11.97	12.7
Ganztägige Tiden:			
Luni-solare Eintagstide	K1	23.93	58.4
Hauptmondtide	O1	25.82	41.5
Hauptsonnentide	P1	24.07	19.3
Langperiodische Tiden:			
14-tägige Mondtide	Mf	327.86	17.2

Gezeiteneffekte

Meeresgezeiten

kompliziert, wegen Land-See-Verteilung und lokalen Resonanzen

Weltrekord: Bucht von Neufundland – Hubhöhe bis 21 m

Gezeitenkraftwerk „La Rance“, Bretagne

Wassergezeiten

Genfer See: bis 2 mm Hub (W-Ende); Chiemsee: bis 1 mm

Boren in Flüssen: Amazonas bis zu 5 m (6.5 m/s), Tsien-tang bis 8 m

Atmosphärengezeiten:

vor allem durch Strahlung, Gravitationseffekt viel kleiner

lunare Perioden im Erdmagnetfeld zu sehen

Gezeiten der festen Erde:

Höhenänderungen (<0.5 m, Schwereänderungen (1/10 000 000 g),

Neigungen (20 msa), Deformationen (< 1/10 000 000),

Spannungen (< 40 hPa), Brunnenspiegel (~ 10 cm) u. a.

Rotationsschwankungen

Triggerung ?

Andere Himmelskörper:

Mondbeben, Io, Europa, Shoemaker-Levy (Roche-Limit)

Gezeitenreibung:

Mond, weitere Resonanzen, Bremsung der Erdrotation

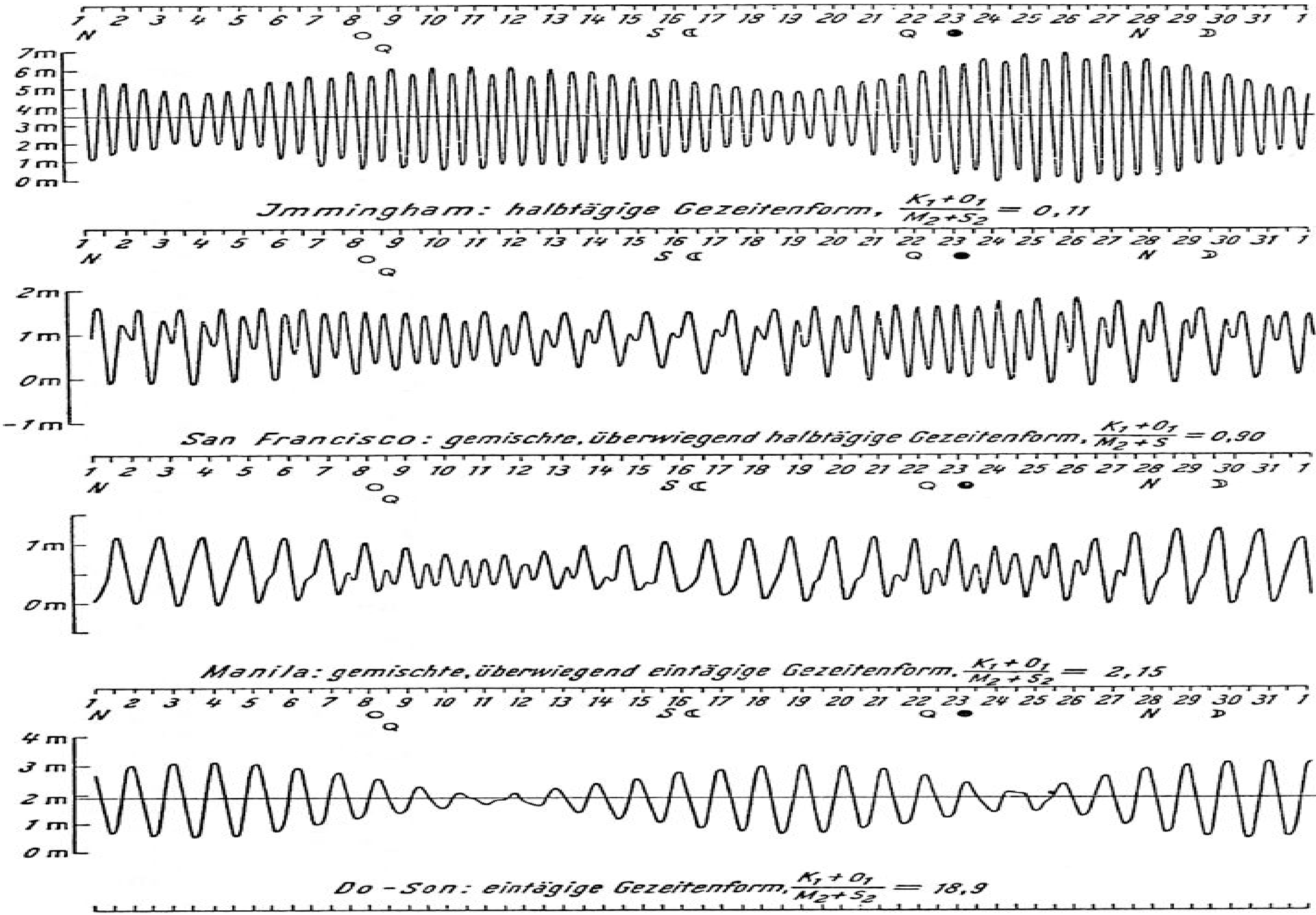

Abb. 35. Gezeitenkurven für den Monat März 1936. (Nach den Deut
schen Gezeitentafeln für das Jahr 1940, Bd. II, Berlin 1939).
○, ☽, ●, ☾: Mondphasen; *N*: größte nördliche, *S*: größte südliche
Deklination des Mondes; *Q*: Äquatordurchgang des Mondes.

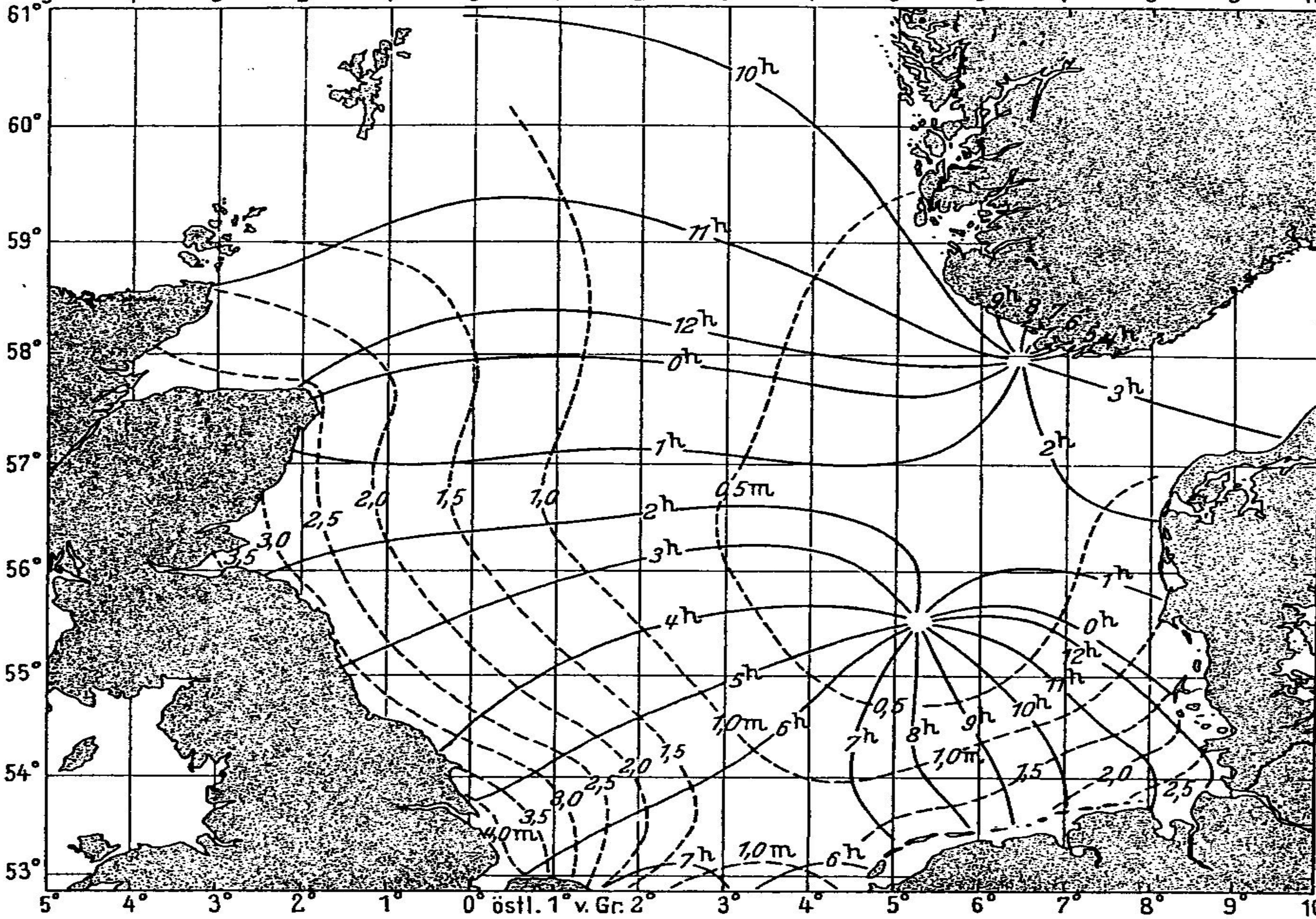

Abb. 48. Gezeitenkarte der Nordsee für die Hauptmondtide M_2 (nach *W. Hansen*). ———: Die mit Uhrzeiten bezifferten Flutstundenlinien (Eintrittszeit des Hochwassers so viel später als der Durchgang des Mondes durch den Meridian von Greenwich). Die gestrichelten Linien sind Linien gleichen mittleren Tidenhubes in Metern.

Gezeiten in Seen und kleineren Meeresbecken

Springtidenhübe

Seen:			
Chiemsee	14 km	W-Ende	0.1 cm
Genfer See	61 km	W-Ende	0.2 cm
Plattensee	77 km	W-Ende	6.5 cm
Erie-See	378 km	W-Ende	8.0 cm
Lake Michigan	550 km	S-Ende	7.3 cm
Lake Superior	650 km	W-Ende	5.9 cm
Baikal-See	665 km		8.2 cm
Meeresbecken:			
Adria	820 km	N-Ende	37.5 cm
Schwarzes Meer	1191 km	E-Ende	8.2 cm
Ostsee	1475 km	W-Ende	4.0 cm
Östl. Mittelmeer	2392 km	E-Ende	11.3 cm
Westl. Mittelmeer	2020 km	E-Ende	15.0 cm
Zum Vergleich:			
Bay of Fundy			2100.0 cm

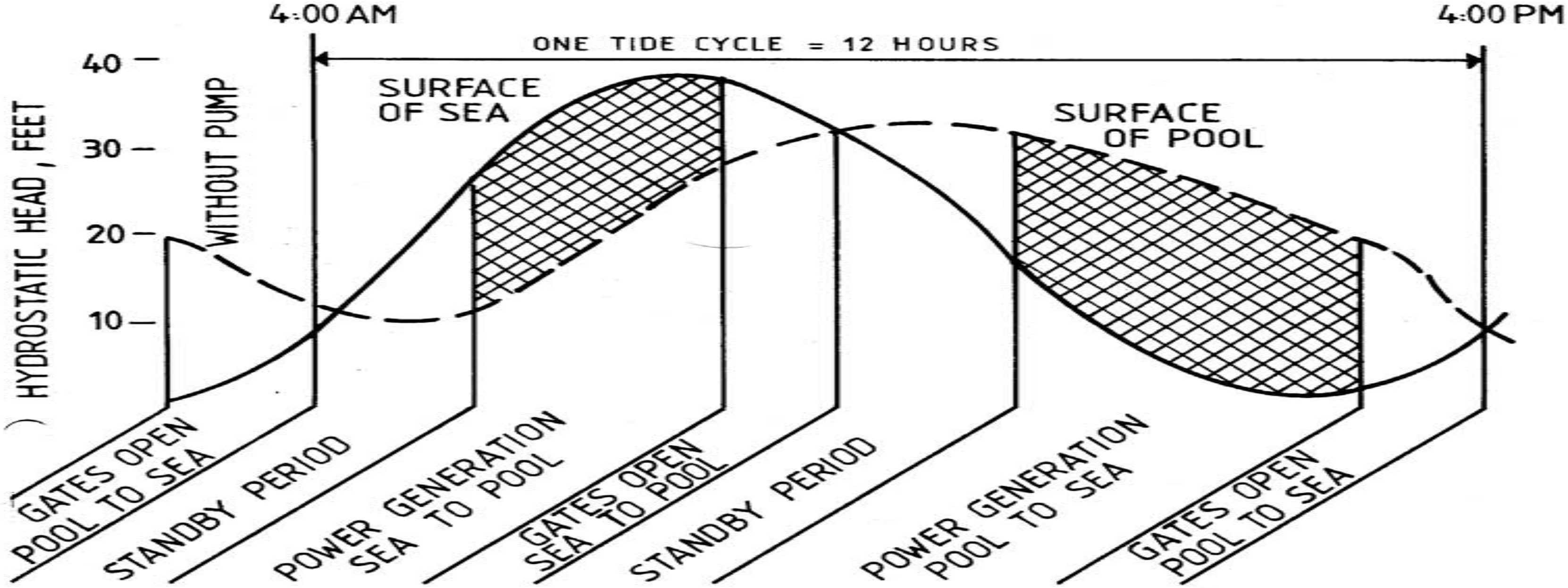

Phases of operation of tidal power plant without pumping

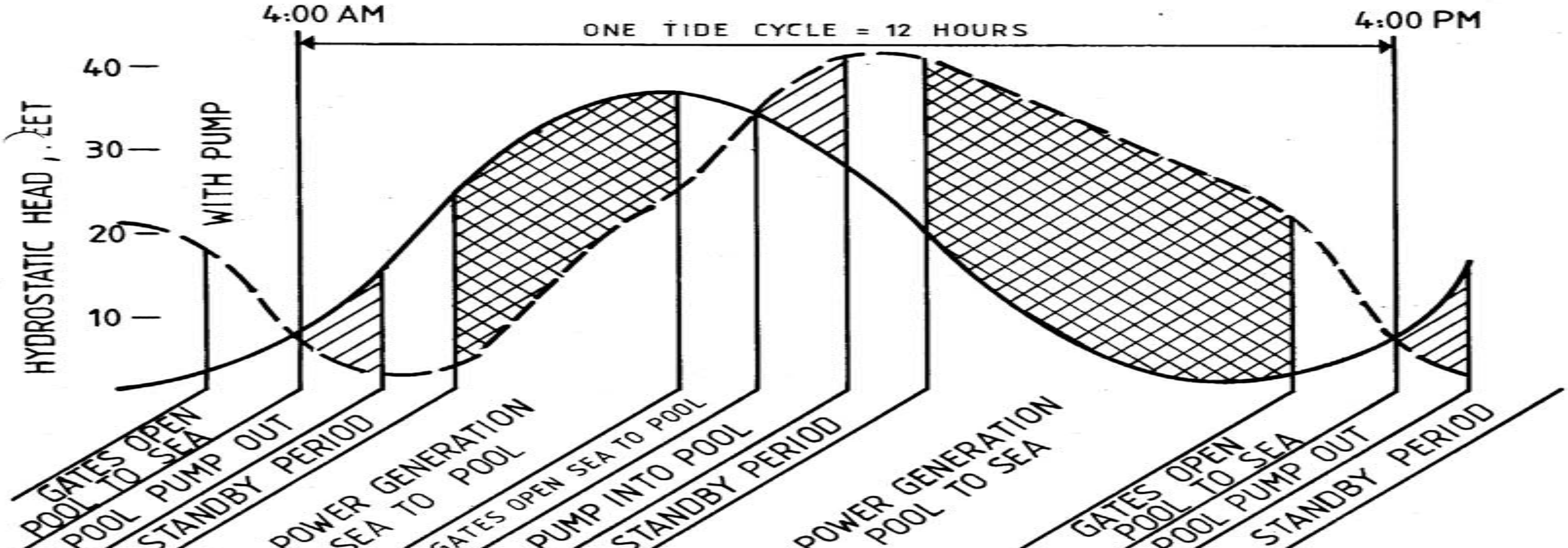

Phases of operation of tidal power plant with pumping

Abb. 55. Bore auf dem Tsien-tang.

The mechanical tide predictor

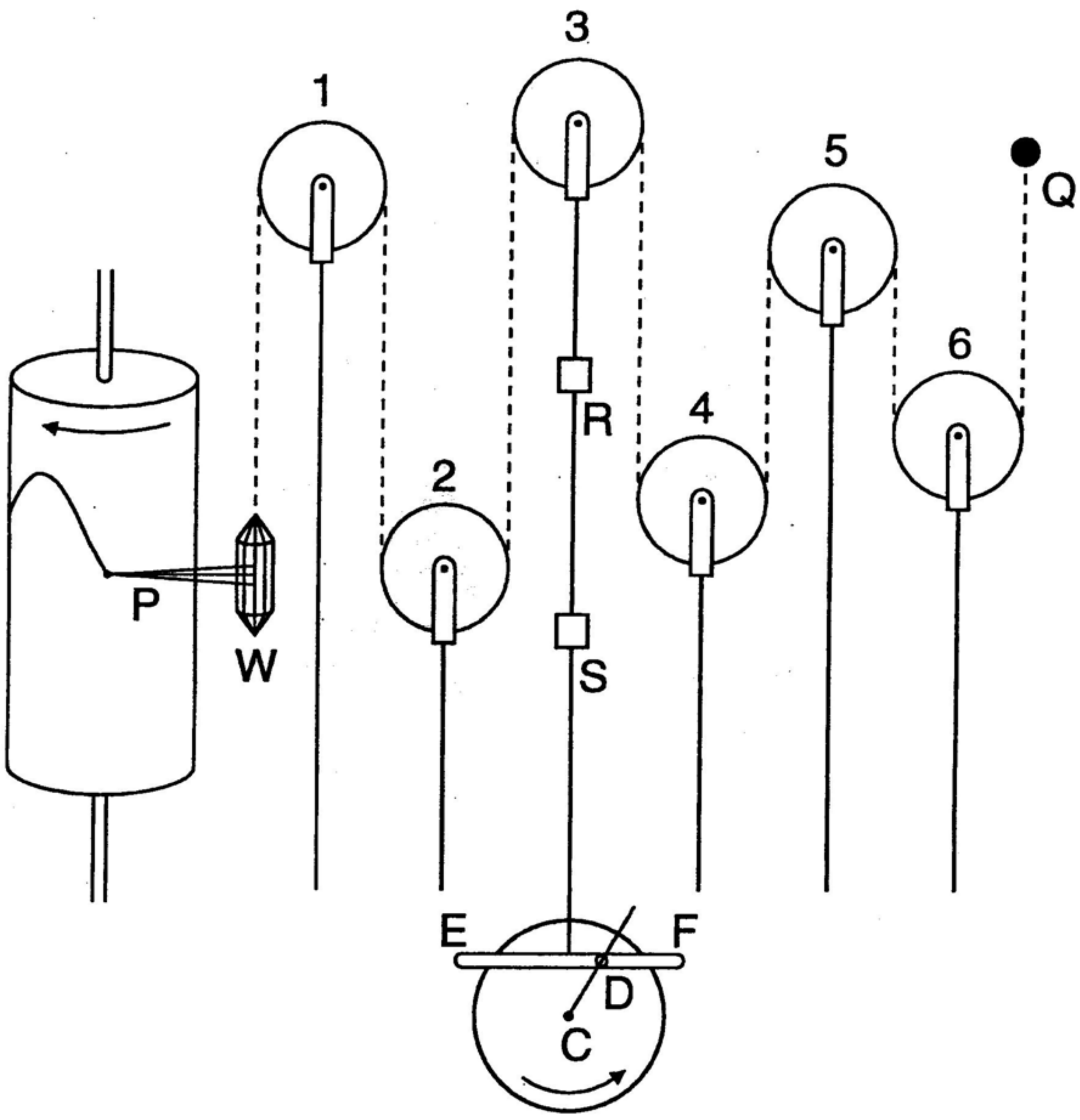

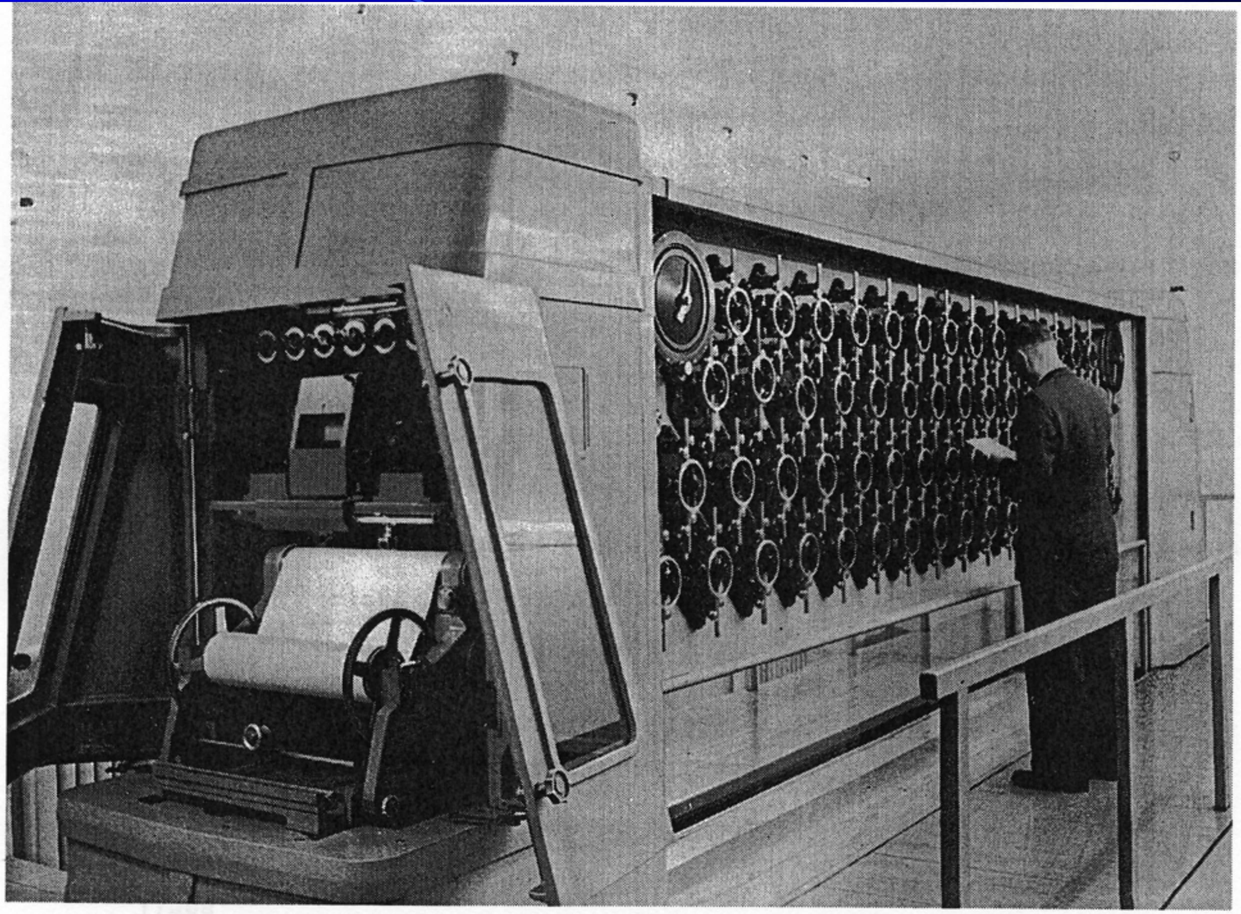

Figure 11.2. The Tide Predicting Machine (*Gezeitenrechenmaschine*) built for the *Deutsche Hydrographische Institut* at Hamburg just before World War II, in its temperature-controlled room. With 62 harmonic components, it was the largest (and heaviest) TPM ever built. The designer, Heinrich Rauschelbach, is standing in front of his machine. (Photograph by courtesy of *Bundesamt für Seeschiffahrt und Hydrographie,* Hamburg.)

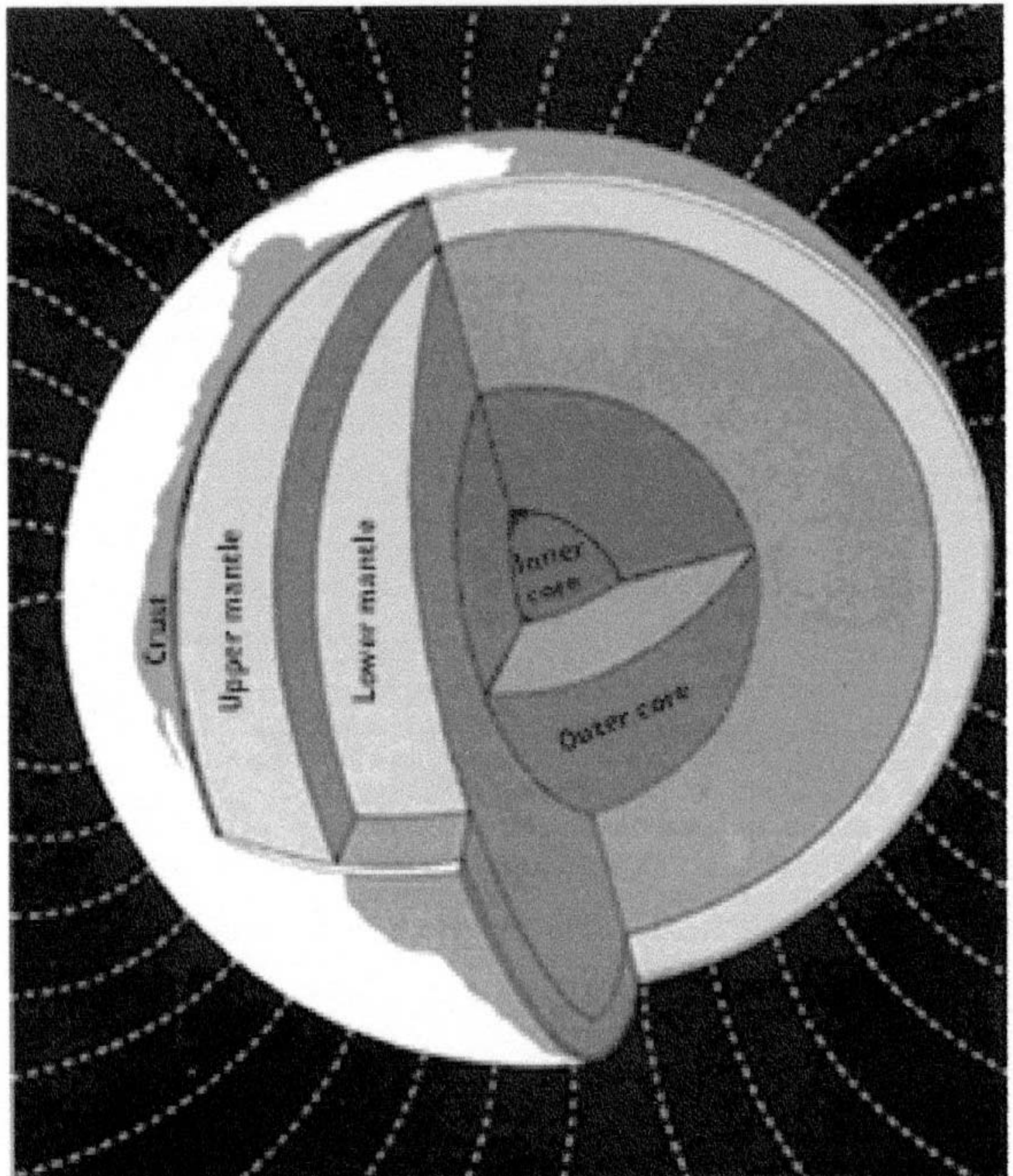
Crust
Upper mantle
Lower mantle
Inner core
Outer core

Messmethoden (stark vereinfacht)

① SCHWEREVARIATIONEN + VERTIKALBESCHLEUNIGUNGEN

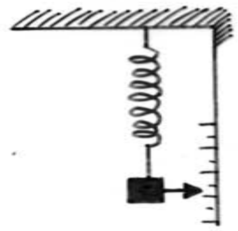

Gravimeter

Vertikal - Seismometer

② NEIGUNGEN + HORIZONTALBESCHLEUNIGUNGEN

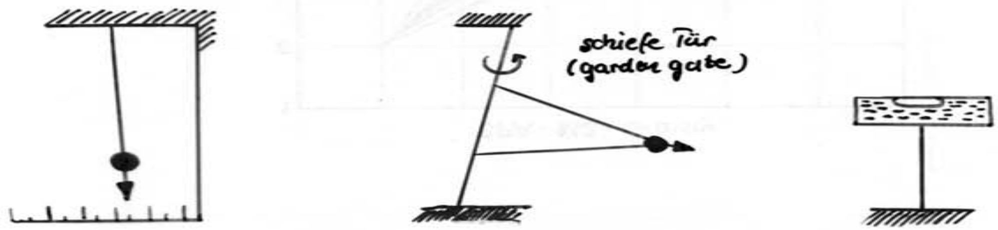

Vertikalpendel

Horizontalpendel und - seismometer

Flüssigkeitslibelle

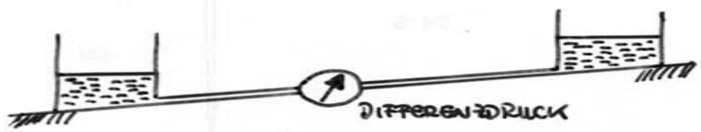

Schlauchwaage { differential pressure, pot and tube, half filled pipe }

③ DEFORMATIONEN

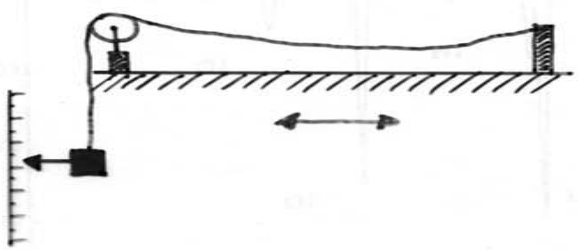

Invar - Draht strainmeter

- extensometer

Quartz - rods
Lasers
Optical Fibers
Dilatometer
Borehole - Strainmeter (Stachin...)

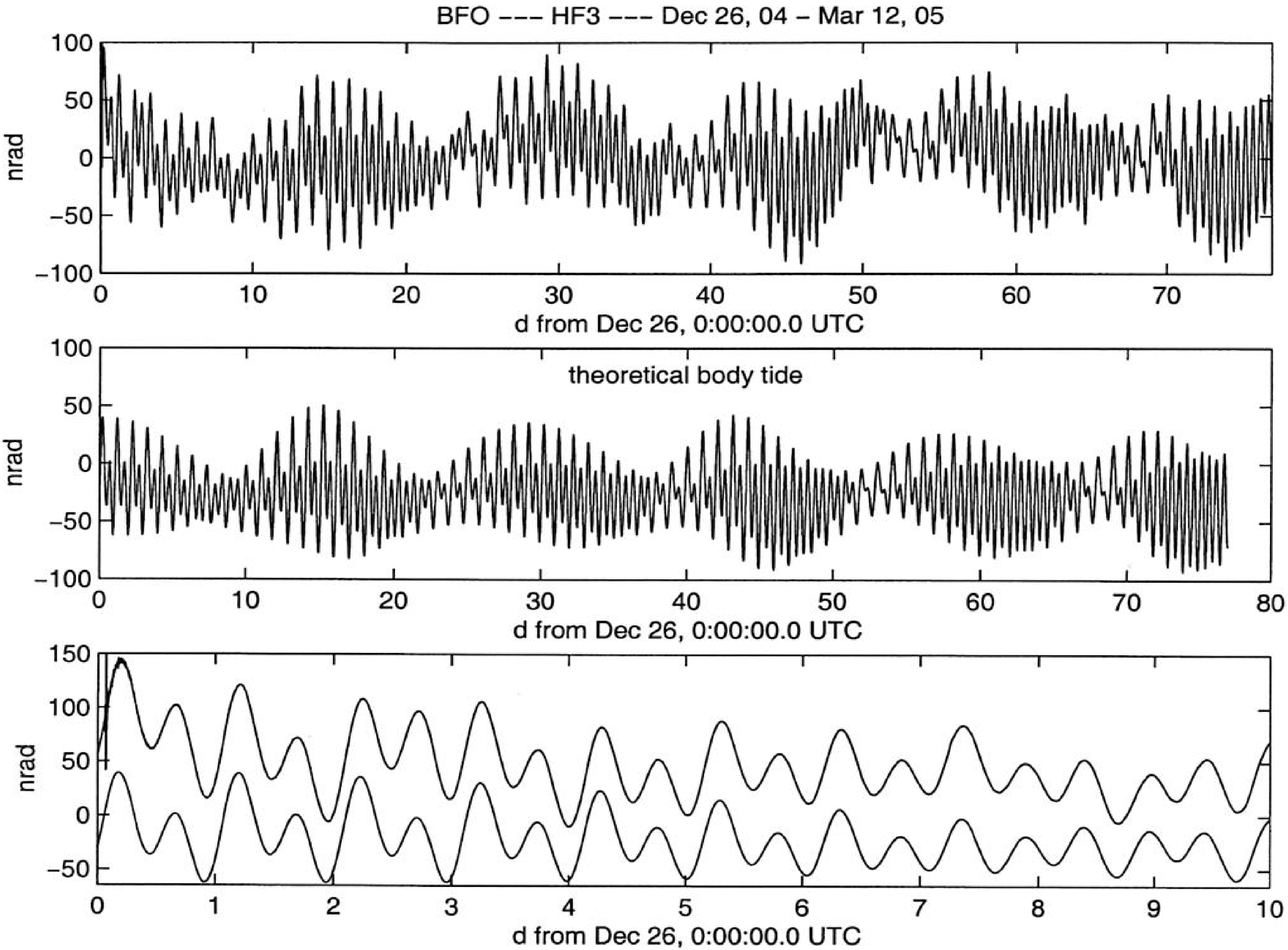
BFO --- HF3 --- Dec 26, 04 – Mar 12, 05
nrad
d from Dec 26, 0:00:00.0 UTC
theoretical body tide
nrad
d from Dec 26, 0:00:00.0 UTC
nrad
d from Dec 26, 0:00:00.0 UTC

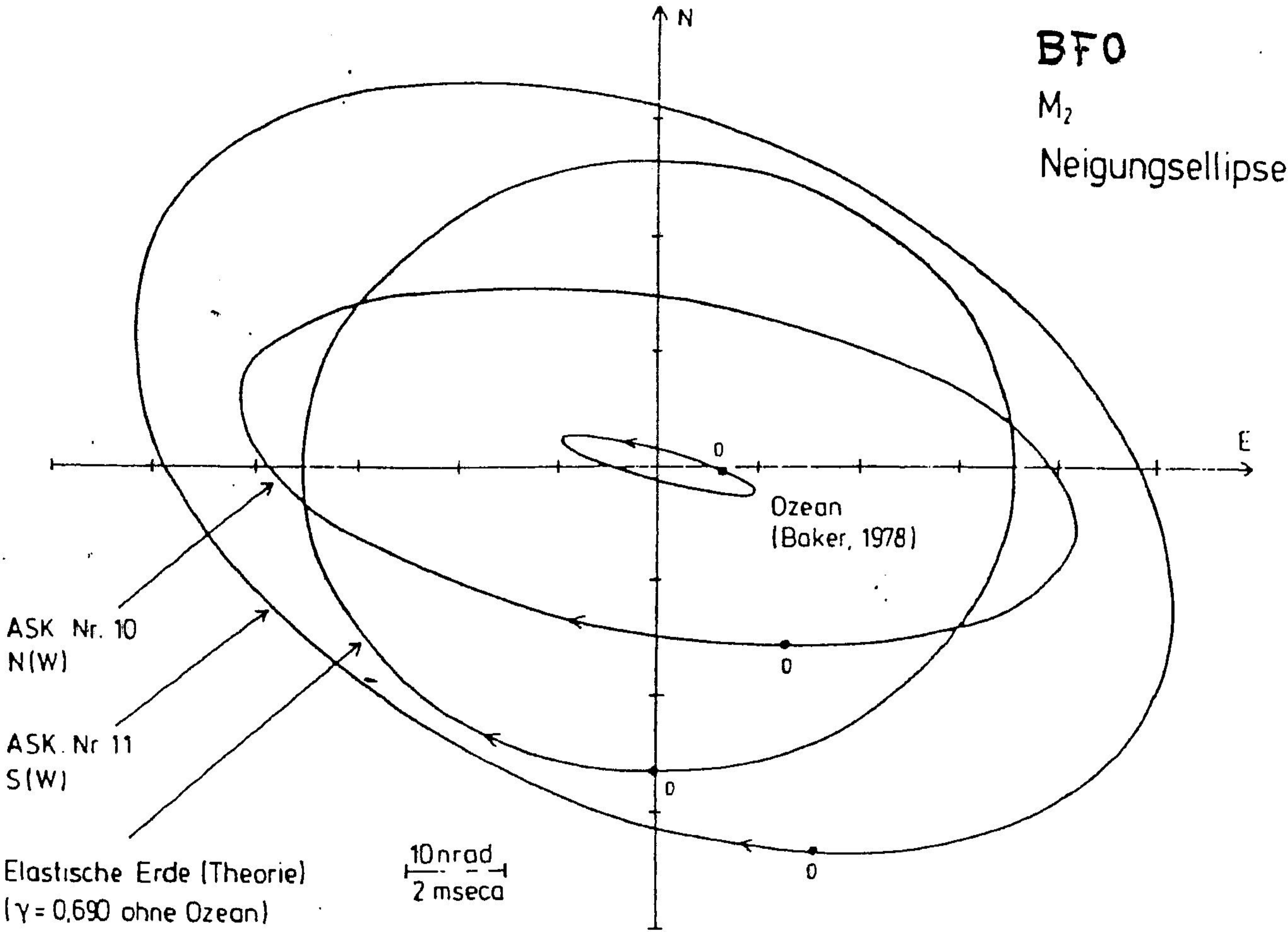

N
E
BFO
M2
Neigungsellipse
0
0
0
0
Ozean
(Baker, 1978)
ASK Nr. 10
N(W)
ASK. Nr 11
S(W)
Elastische Erde (Theorie)
(γ = 0,690 ohne Ozean)
10 nrad
2 mseca

Zaske et al., 2000

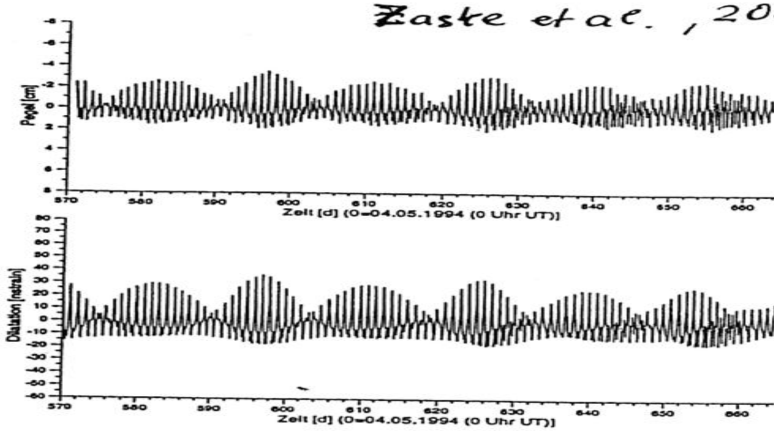

Figure 16: (a) High-pass filtered and air pressure reduced well level data and (b) theoretical tidal dilatation calculated for Soultz-sous-Forêts using the Tamura potential. The air pressure reduction was done using a barometric efficiency of 0.575, determined by the earth tide analysis.

Kulessa et al. (2003)

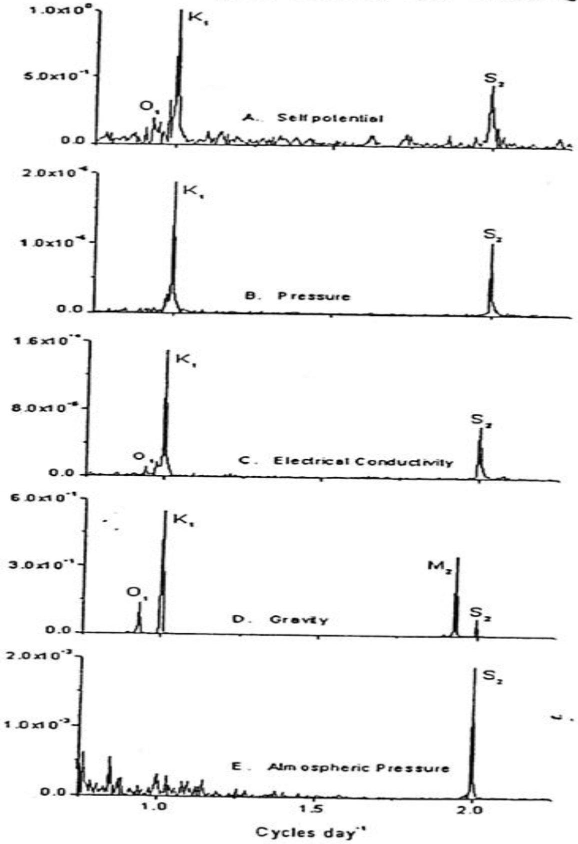

re 2. Fourier power spectra for the 1996–97 winter. O_1, S_2, and M_2 respectively represent the luni-solar al, principal lunar diurnal, principal solar semi-diurnal, principal lunar semi-diurnal components.

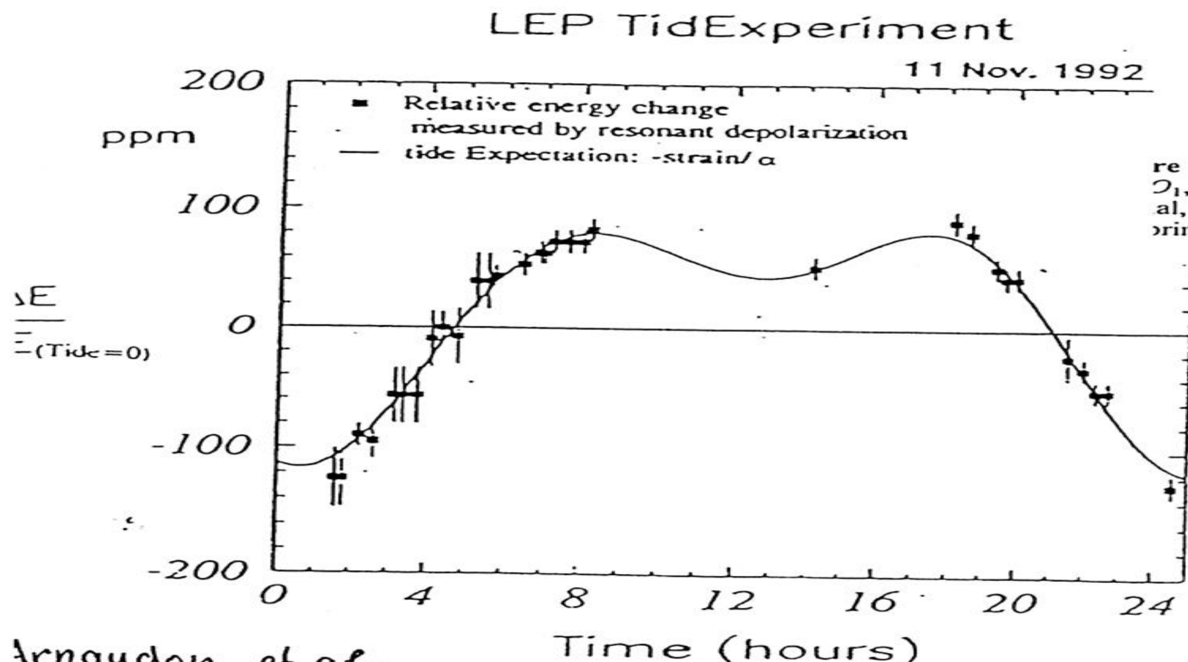

Arnaudon et.al.

Westerhaus & Zschau (2001)
North Anatolian Fault, Turkey

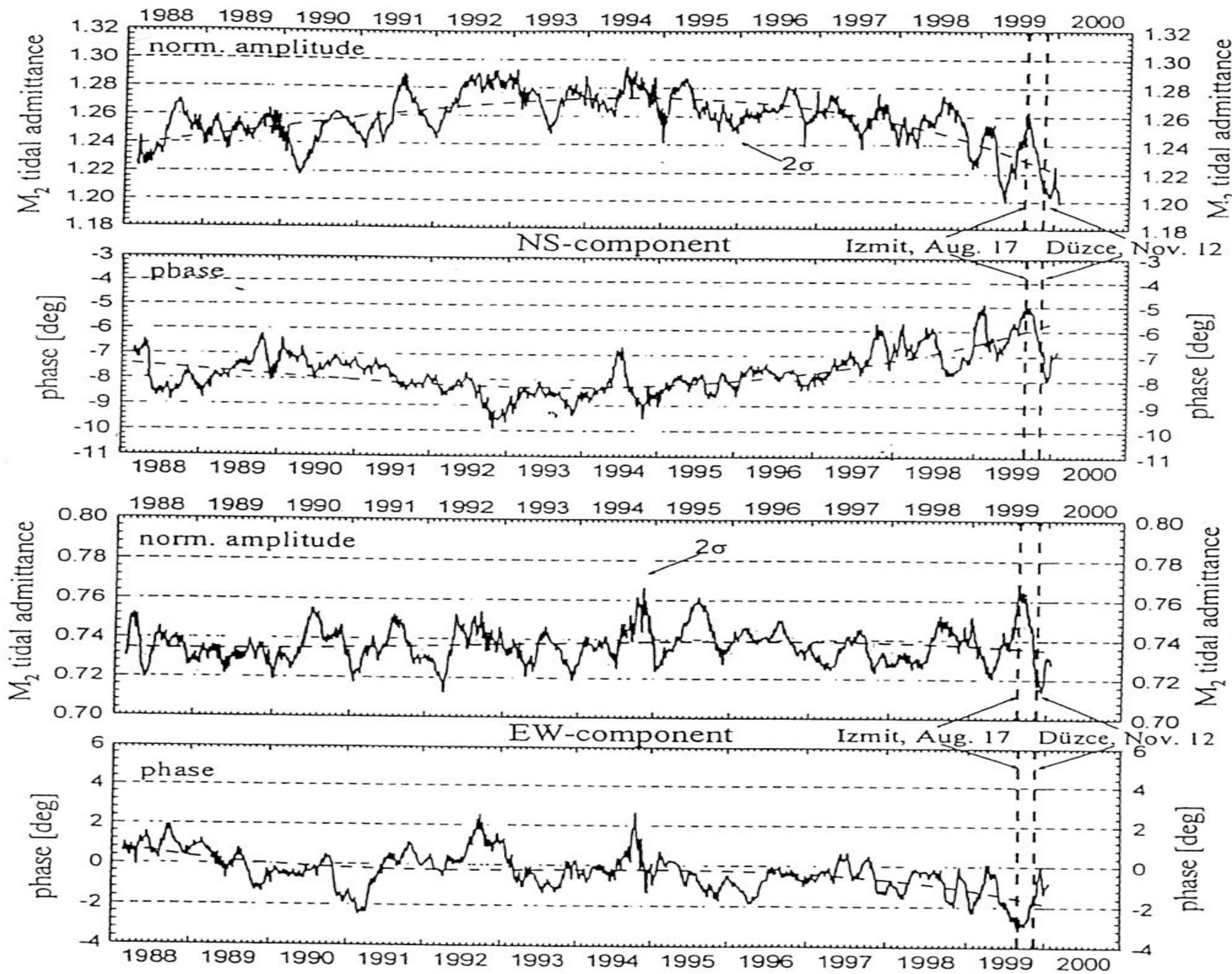

Fig. 4. Variations with annual and semi-annual periods are a common feature of the M2-tidal tilt response function at site SAM. No seismically induced anomalies can be resolved against this background. A long term trend, not seen in the component (EW) parallel to the main fault, is supposed to be related to geology; a connection to the 1999 earthquakes, however, remains speculative.

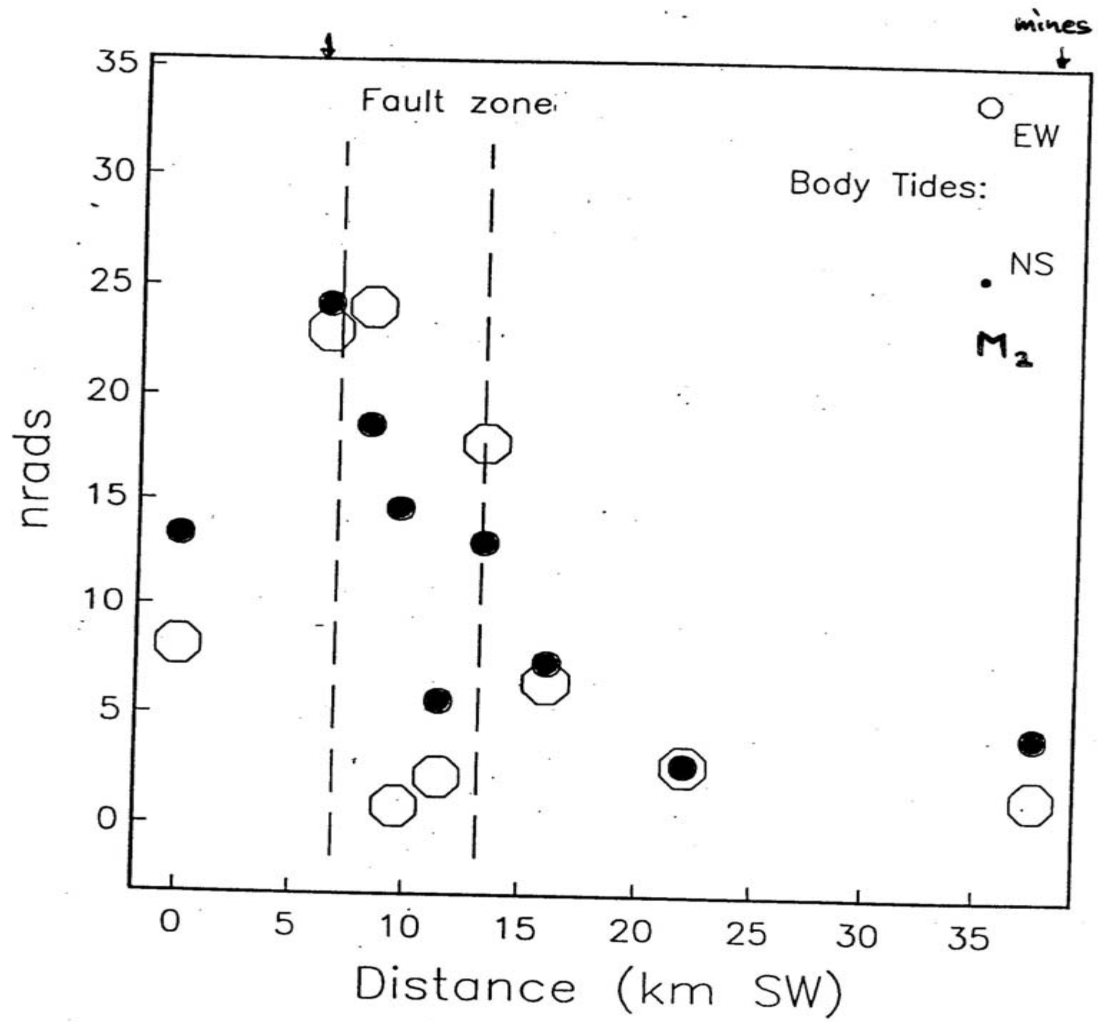
mines
Fault zone
EW
Body Tides:
NS
M_2
nrads
35
30
25
20
15
10
5
0
0
5
10
15
20
25
30
35
Distance (km SW)

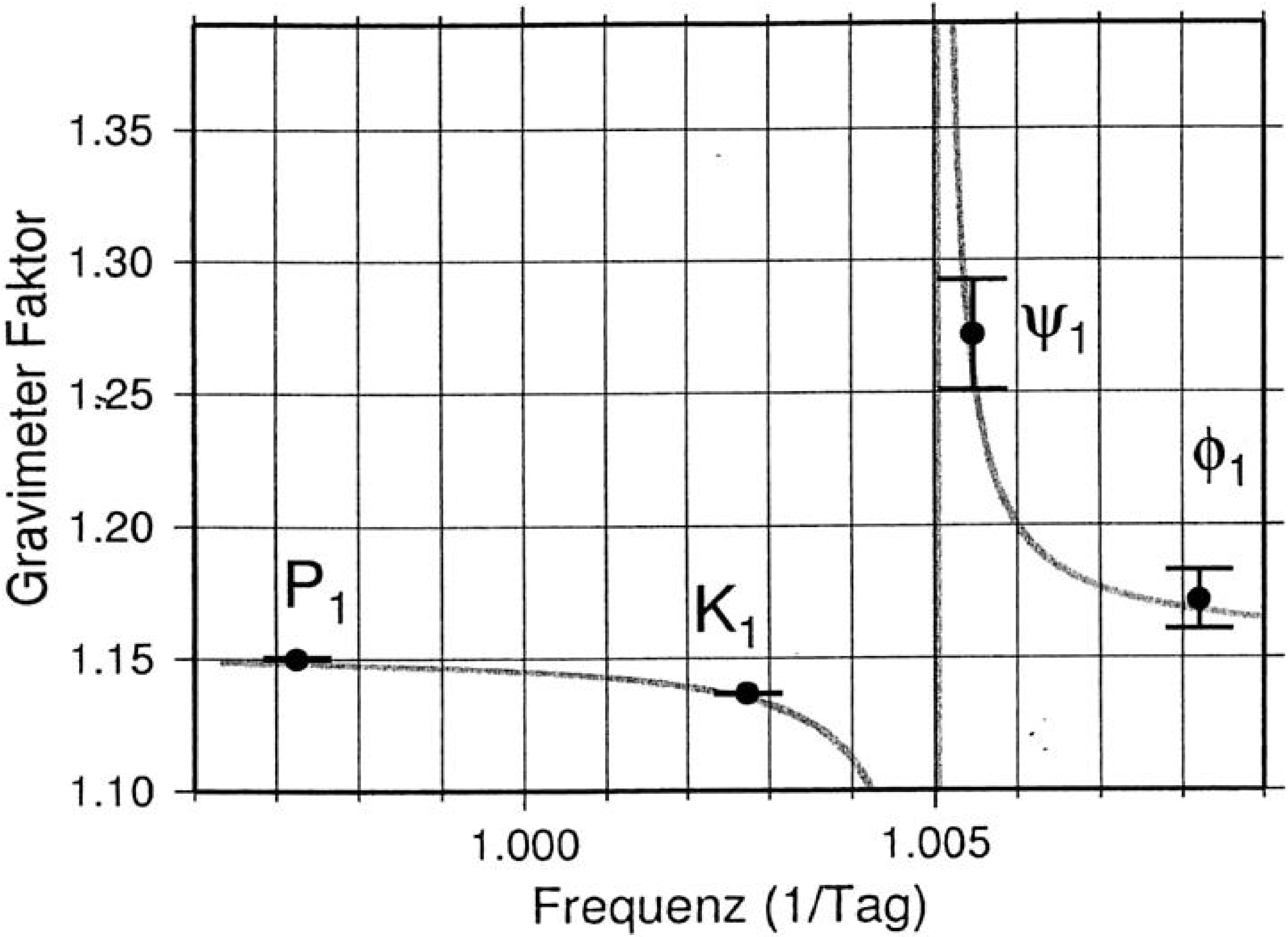

Gravimeter Faktor
1.35
1.30
1.25
1.20
1.15
1.10
1.000
1.005
Frequenz (1/Tag)
P1
K1
Ψ1
φ1

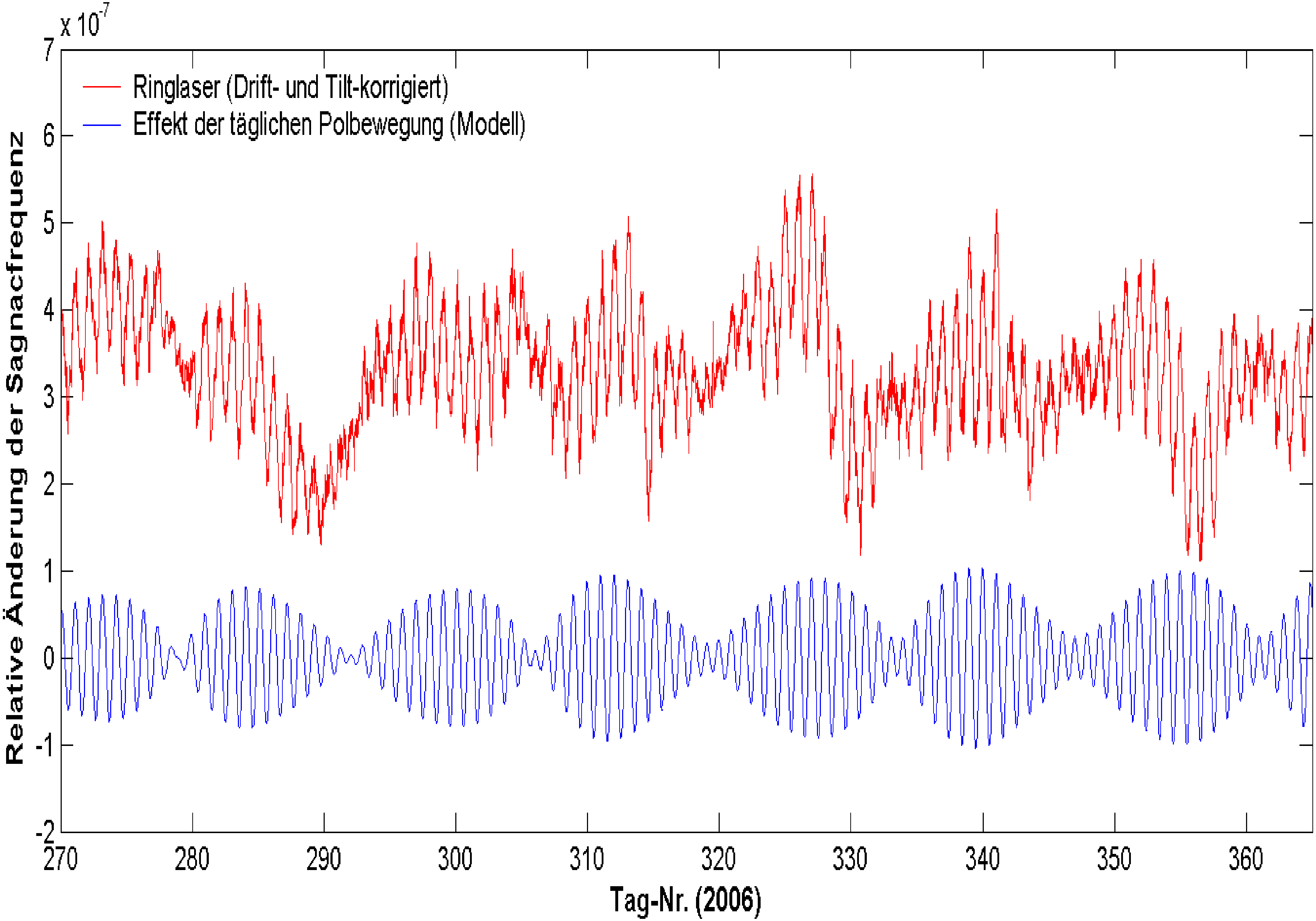

x 10^-7
7
6
5
4
3
2
1
0
-1
-2
Ringlaser (Drift- und Tilt-korrigiert)
Effekt der täglichen Polbewegung (Modell)
Relative Änderung der Sagnacfrequenz
270
280
290
300
310
320
330
340
350
360
Tag-Nr. (2006)

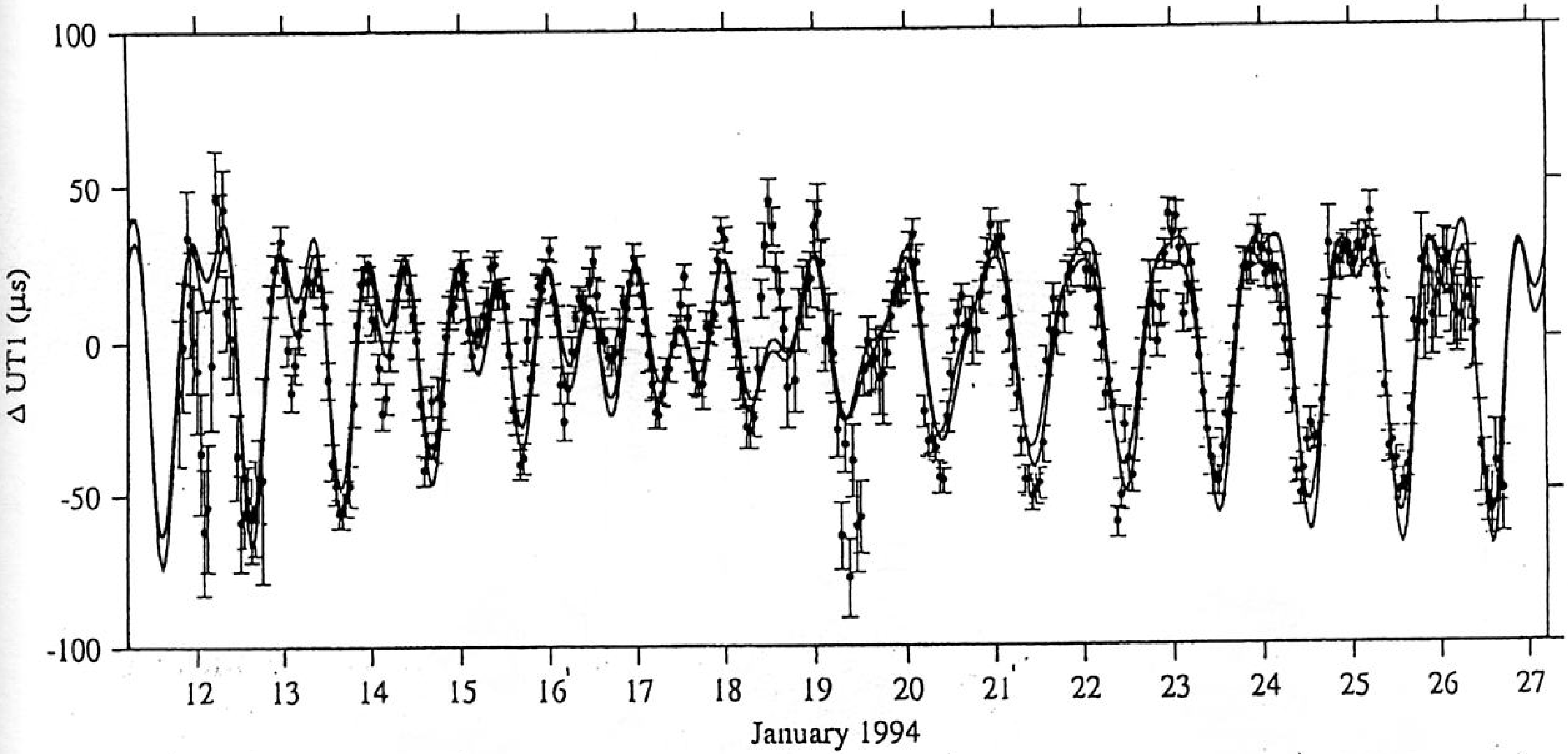

Figure 15.4. Fluctuations in Universal Time (UT1) recorded hourly by a VLBI network from 11 to 26 January, 1994 – spots with standard error limits – compared with two similar syntheses computed from independent models of four diurnal and four semidiurnal tide constituents – continuous lines. Vertical scale in microseconds. A low-order polynomial trend has been subtracted from all data. (Courtesy of R.D. Ray.)

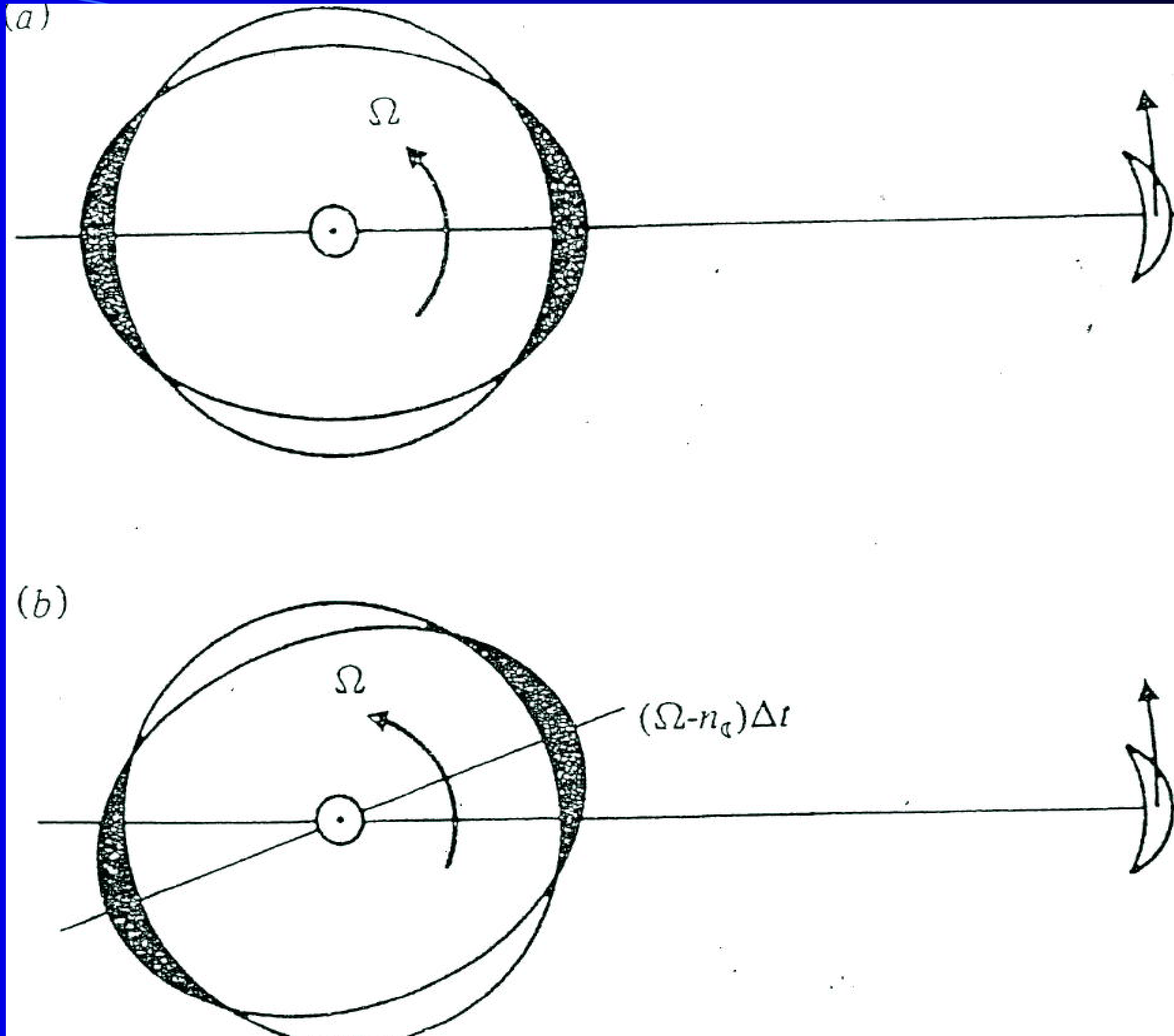
(a)
Ω
(b)
Ω
(Ω-n☾)Δt

SCIENCE, VOL. 203, 2 MARCH 1979

Melting of Io by Tidal Dissipation

Abstract. *The dissipation of tidal energy in Jupiter's satellite Io is likely to have melted a major fraction of the mass. Consequences of a largely molten interior may be evident in pictures of Io's surface returned by Voyager I.*

S. J. PEALE

Department of Physics,
University of California,
Santa Barbara 93106

P. CASSEN
R. T. REYNOLDS

Theoretical and Planetary Studies
Branch, NASA-Ames Research Center,
Moffett Field, California 94035

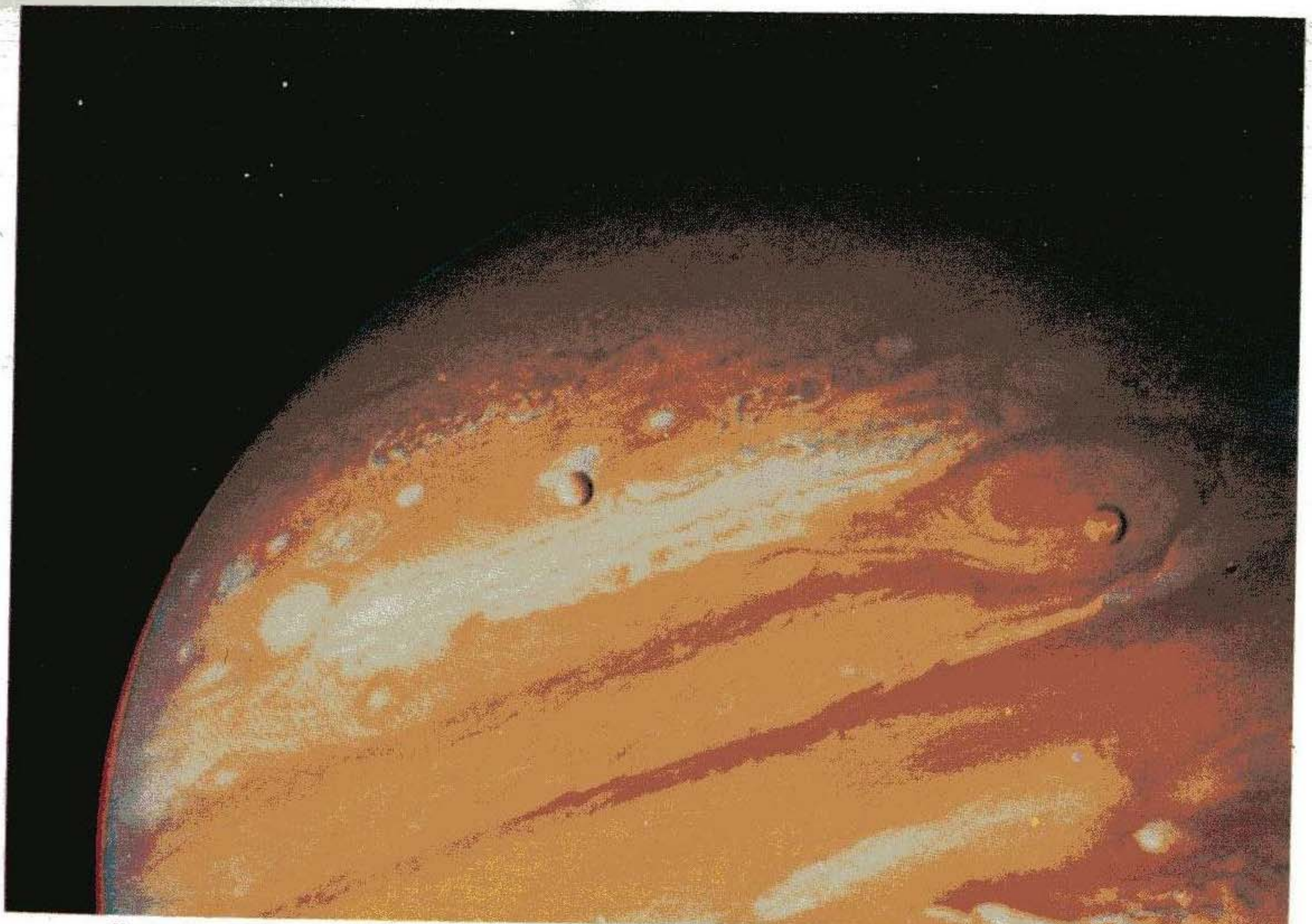

Voyager I took this photo of Jupiter and two of its satellites (Io, left, and Europa) on February 13, 1979. Io is about 350,000 km (220,000 miles) above Jupiter's Great Red Spot: Europa is about 600,000 km (375,000 miles) above Jupiter's clouds. Although both satellites have about the same brightness, Io's color is very different from Europa's. Io's equatorial region shows two types of material—dark orange, broken by several bright spots—producing a mottled appearance. The poles are darker and reddish. Preliminary evidence suggests color variations within and between the polar regions. Io's surface composition is unknown, but scientists believe it may be a mixture of salts and sulfur. Europa is less strongly colored, although still relatively dark at short wavelengths. Markings on Europa are less evident than on the other satellites, although this picture shows darker regions toward the trailing half of the visible disk. Jupiter is about 20 million km (12.4 million miles) from the spacecraft. At this resolution (about 400 km or 250 miles) there is evidence of circular motion in Jupiter's atmosphere. While the dominant large-scale motions are west-to-east, small-scale movement includes eddy-like circulation within and between the bands. This photo was assembled from three black and white negatives by the Image Processing Lab at Jet Propulsion Laboratory. JPL manages and controls the Voyager project for NASA's Office of Space Science.

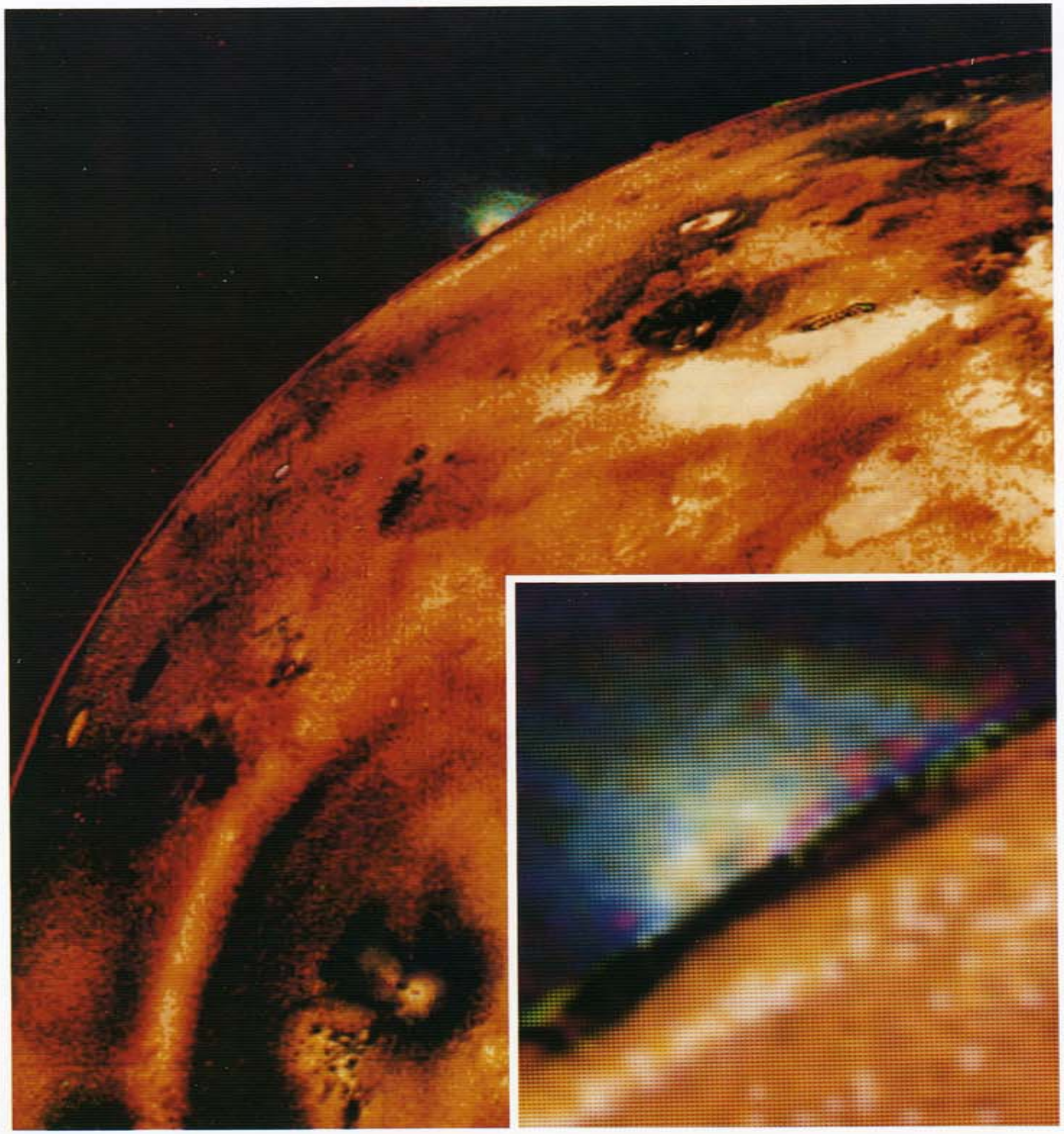

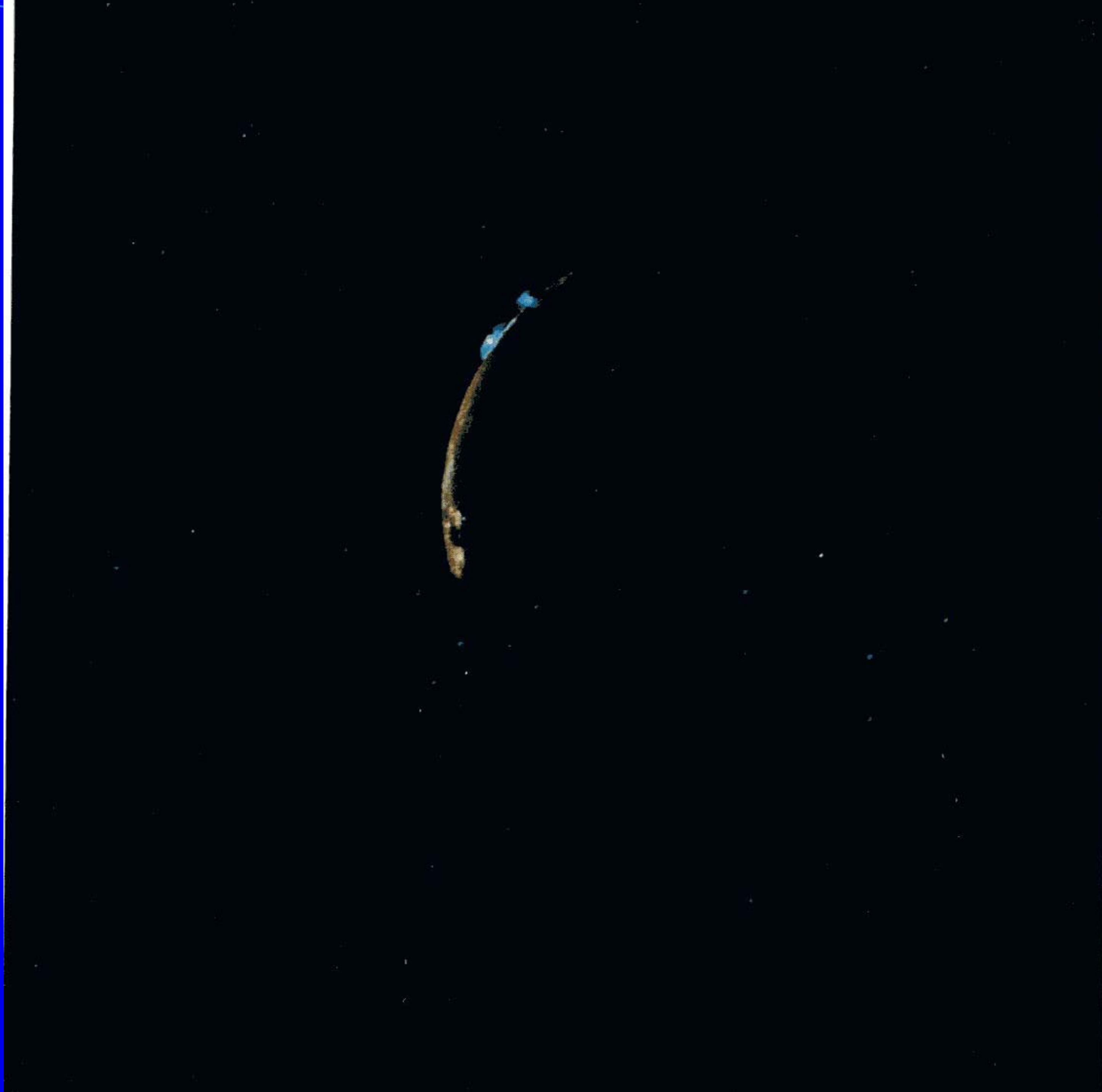

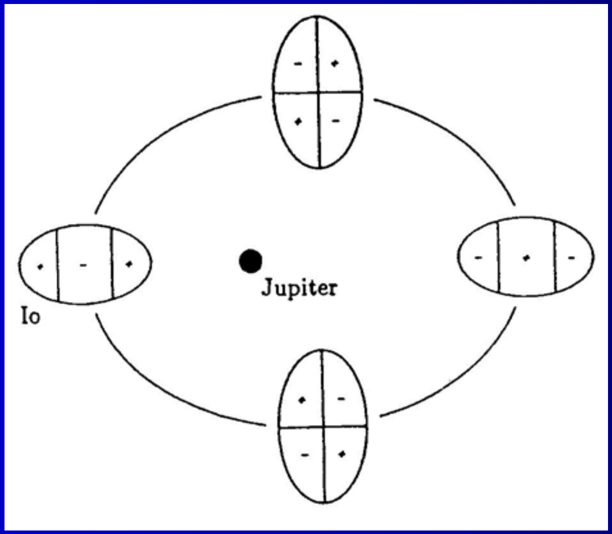

Jupiter
Io

測地学会誌，第47巻，第1号
(2001)，501-507頁

Journal of the Geodetic Society of Japan
Vol. 47, No. 1, (2001), pp. 501-507

Europa's Tides and Possible Hidden Liquid Ocean–With New Simulations on Different Orbit Configurations and Non-Global Ocean Basins

Xiaoping Wu*, Yoaz Bar-Sever, William Folkner, James Williams and James Zumberge

Jet Propulsion Laboratory, California Institute of Technology,
MS 238-600, 4800 Oak Grove Drive, Pasadena, CA 91109, U.S.A.

(Received September 27, 2000; Revised December 26, 2000; Accepted January 3, 2001)

Abstract

Observations of Europa suggest that the Jovian satellite may have a liquid water ocean under its surface ice shell. One possible way to detect the ocean is to measure tidal gravity and topography variations by precise Doppler tracking and laser altimetry during the planned Europa Orbiter Mission. Another way to detect the global ocean is to measure the likely difference between the 3.55-day libration amplitudes of the ice shell and rocky mantle beyond statistical doubt.

Covariance analyses are carried out to determine measurement accuracies for k_2, gravity fields and librations in longitude for the ice shell and rocky mantle, epoch orbit states and other parameters. The analyses use 15 days of X-band two-way Doppler tracking from 2 or 3 Earth stations with various possible orbital altitudes and inclinations. The uncertainty obtained for the epoch radial orbit position here can also be used to assess altimeter measurement accuracy. The possibility of non-global ocean basins and its consequence in tidal gravity measurements are also discussed.

Fluid Core Size of Mars from Detection of the Solar Tide

C. F. Yoder,* A. S. Konopliv,* D. N. Yuan, E. M. Standish, W. M. Folkner

SCIENCE VOL 300 11 APR

The solar tidal deformation of Mars, measured by its k_2 potential Love number, has been obtained from an analysis of Mars Global Surveyor radio tracking. The observed k_2 of 0.153 ± 0.017 is large enough to rule out a solid iron core and so indicates that at least the outer part of the core is liquid. The inferred core radius is between 1520 and 1840 kilometers and is independent of many interior properties, although partial melt of the mantle is one factor that could reduce core size. Ice-cap mass changes can be deduced from the seasonal variations in air pressure and the odd gravity harmonic J_3, given knowledge of cap mass distribution with latitude. The south cap seasonal mass change is about 30 to 40% larger than that of the north cap.

Danke für‘s Zuhören und Zusehen

Ich bin gerne bereit, Fragen zu beantworten

HORSFALL-Tiltmeter

Schiltach

l = 270m   φ = N 25°14'E
baseline = 170m

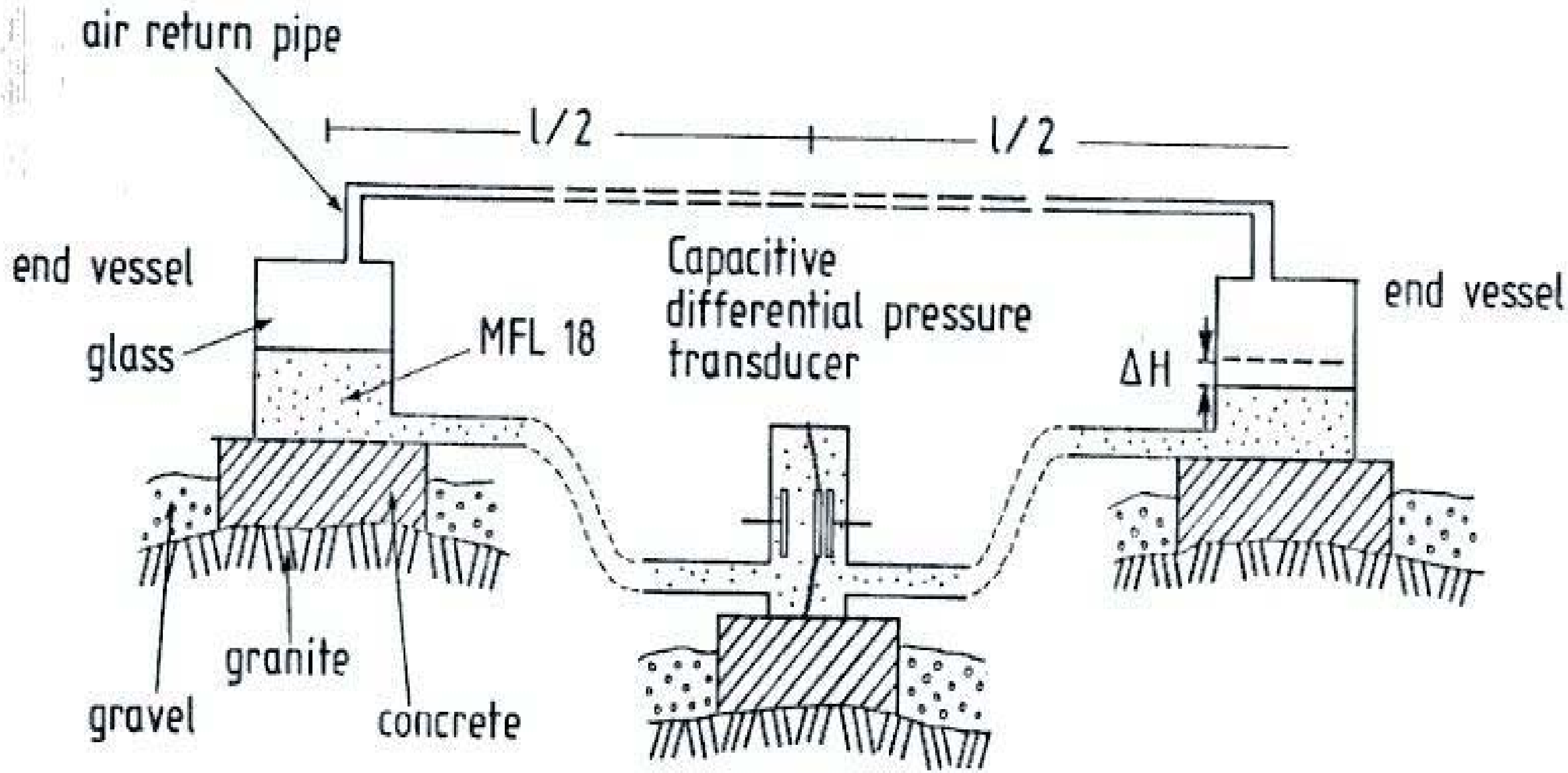

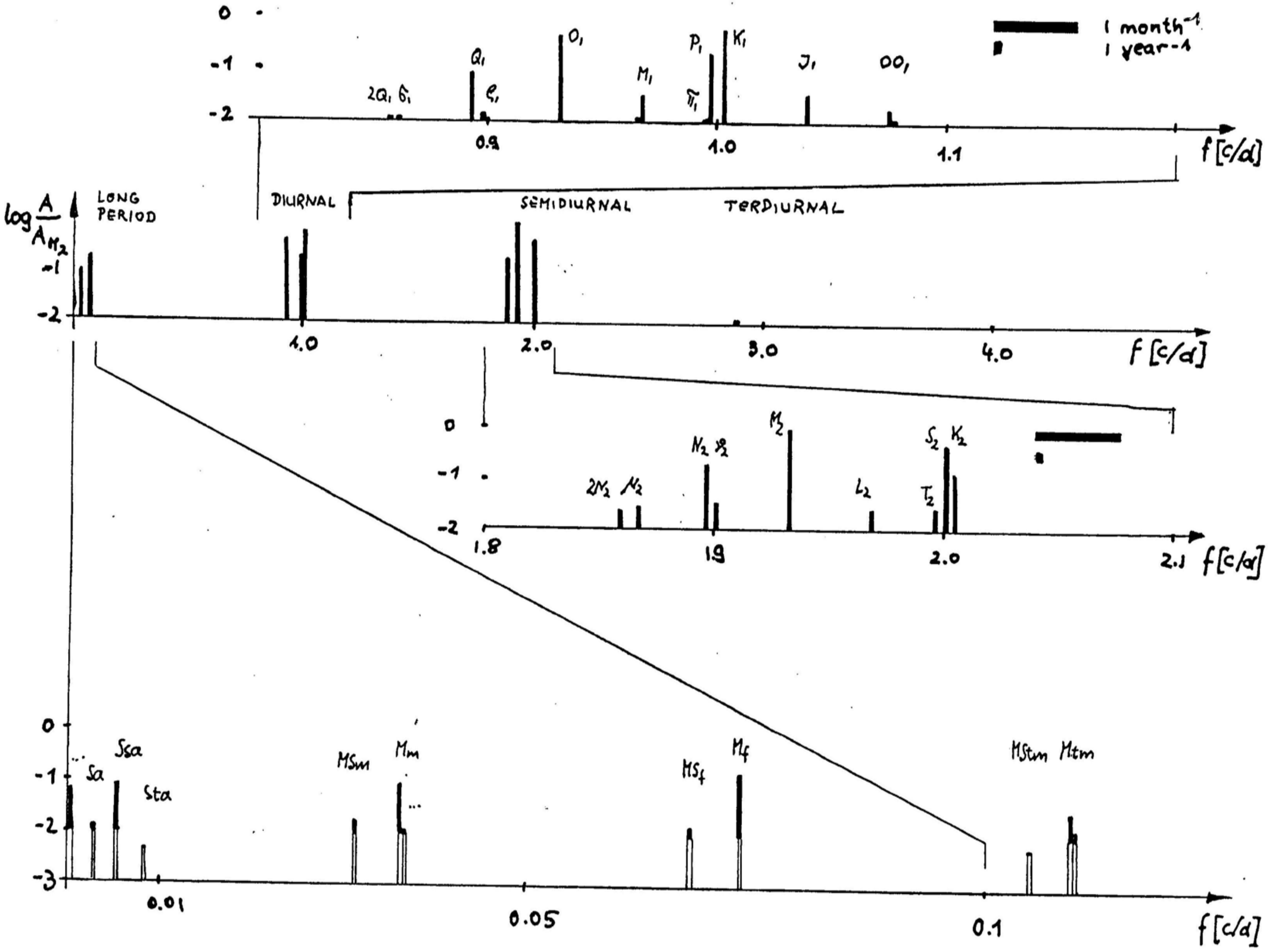

1 month⁻¹
1 year⁻¹
2Q₁ σ₁
Q₁
ρ₁
O₁
M₁
π₁
P₁
K₁
J₁
OO₁
0.9
1.0
1.1
f [c/d]
log A/A_{M₂}
LONG PERIOD
DIURNAL
SEMIDIURNAL
TERDIURNAL
1.0
2.0
3.0
4.0
f [c/d]
2N₂ μ₂
N₂ ν₂
M₂
L₂
T₂
S₂ K₂
1.8
1.9
2.0
2.1
f [c/d]
Sa
Ssa
Sta
MSm
Mm
MSf
Mf
MStm
Mtm
0.01
0.05
0.1
f [c/d]

Schematical Interpretation of Tidal Signal

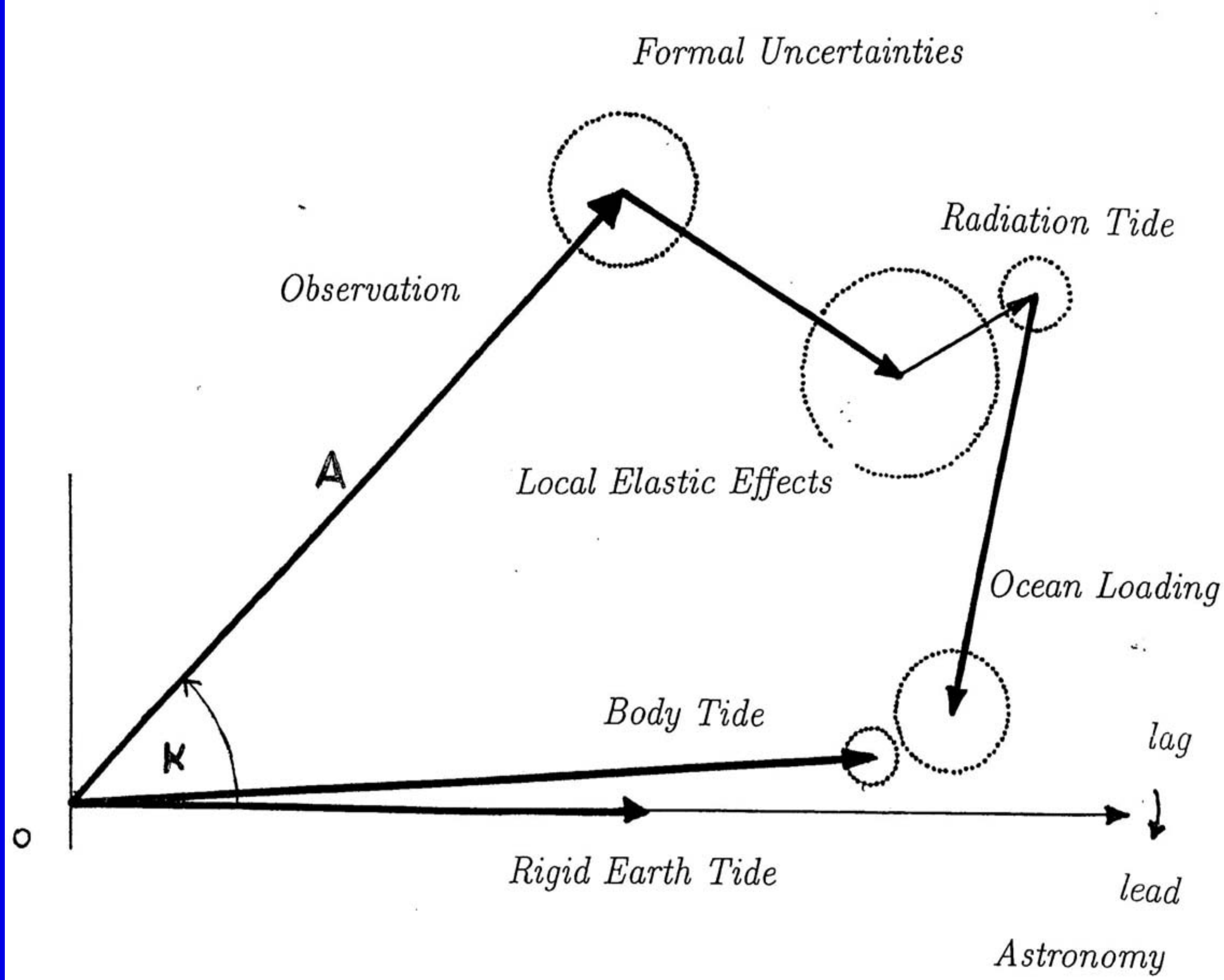

Auflösung

- Schwerevariationen bzw. Vertikalbeschleunigungen

$$\frac{\Delta g}{g} = 10^{-12} = \frac{1}{1000000000000} \qquad (1)$$

Ständig angeregte elastische Resonanzen der Erde, durch Atmosphärendruckschwankungen (?) im Periodenbereich von 150 - 500 Sekunden.
Entspricht Schwerebeschleunigung durch einen Singvogel (100 g) im Abstand von 1 m
Beispiel: BFO LCR-ET-19 gravimeter

- Neigungen und Deformationen

$$\frac{\Delta l}{L} = 10^{-11} = \frac{1}{100000000000} \qquad (2)$$

Torsionale Grundschwingung (Verdrillung) der Erde mit 44 Minuten Periode, nach den stärksten Erdbeben.
Diese relativen Verschiebungen entsprechen:
— 4 mm auf dem Mond von BRD aus gesehen,
— Papierblattdicke (1/10 mm) auf Strecke BRD - Beijing,
— 1/100 mm auf Strecke Zürich - Kopenhagen
— 1/1000 mm auf Strecke Göttingen - Hannover
Beispiel: BFO (Widmer u. a.)

BFO

Cleft - Strainmeter

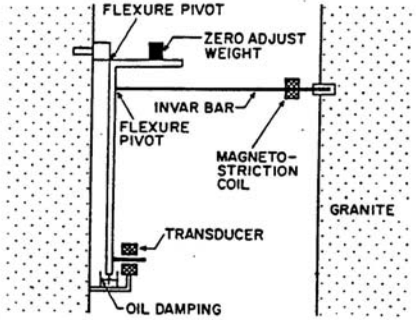

Figure 2 Schematic diagram of the cleft strainmeter.

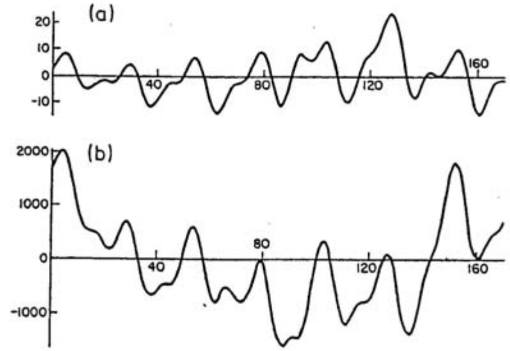

b) One week segments of tidal data from the D37 (a) and cleft (b) strainmeters respectively.

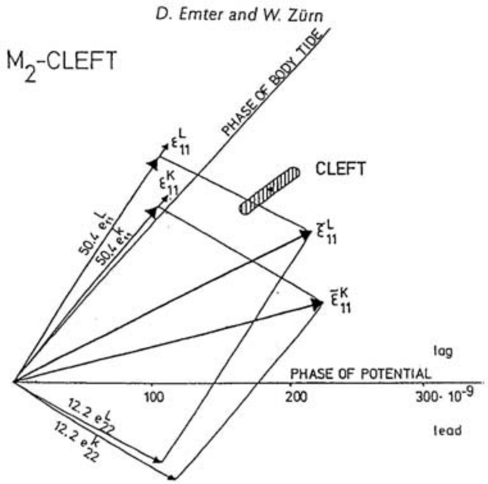

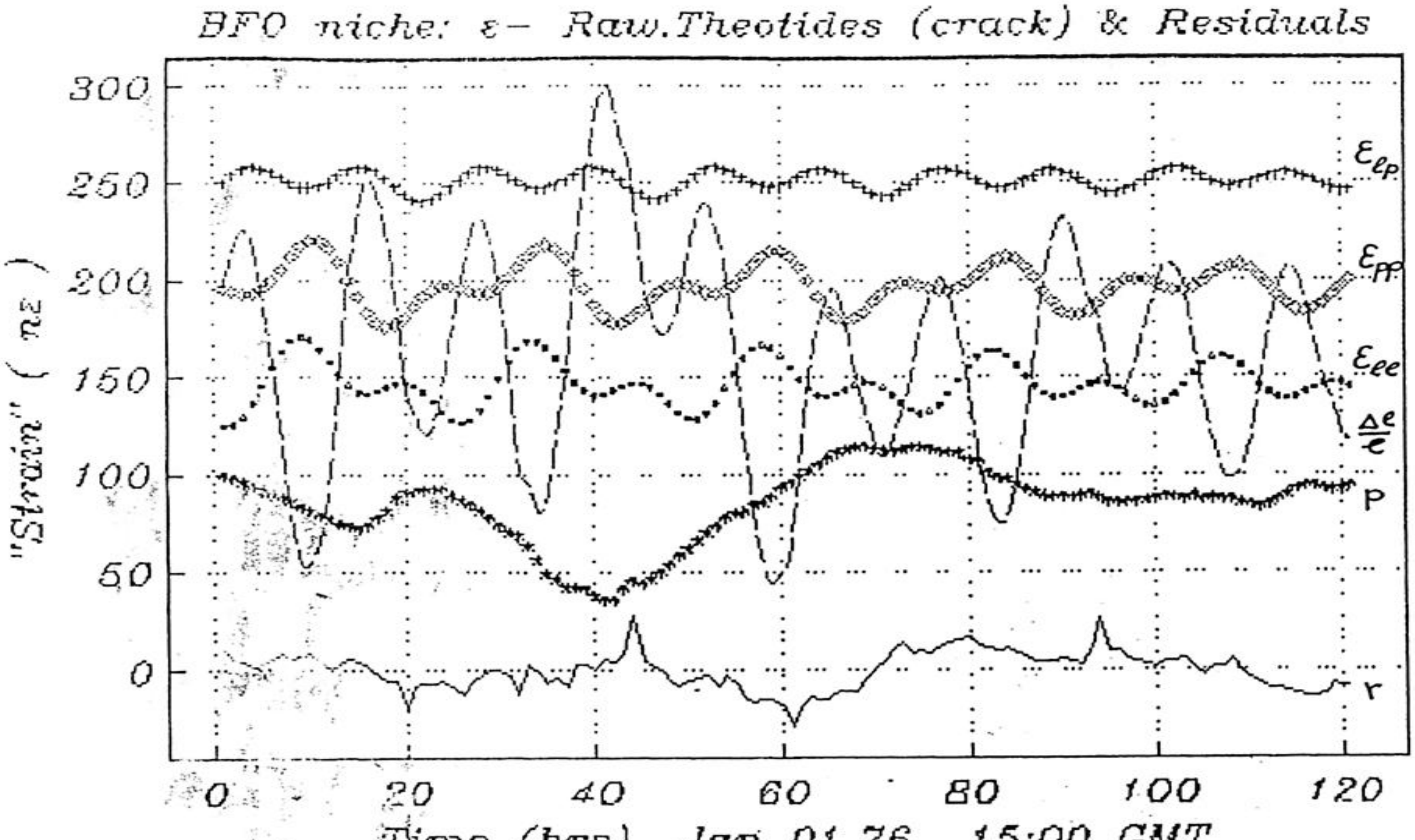

coefficient	units	stand.dev.
$A_{pp} = -2.05$	–	± 0.11
$A_{ll} = -2.39$	–	± 0.11
$A_{lp} = +4.77$	–	± 0.20
$A_p = -5.56$	$n\epsilon/hPa$	± 0.25
$a_1 = -0.073$	$n\epsilon/hr$	± 0.10
$a_2 = -0.0096$	$n\epsilon/hr^2$	± 0.0008

$$\frac{\Delta l}{l_0(t)} = A_{pp} \cdot \epsilon_{pp}(t) + A_{ll} \cdot \epsilon_{ll}(t) + A_{lp} \cdot \epsilon_{lp}(t) + A_p \cdot p(t) + a_0 + a_1 t + a_2 t^2.$$

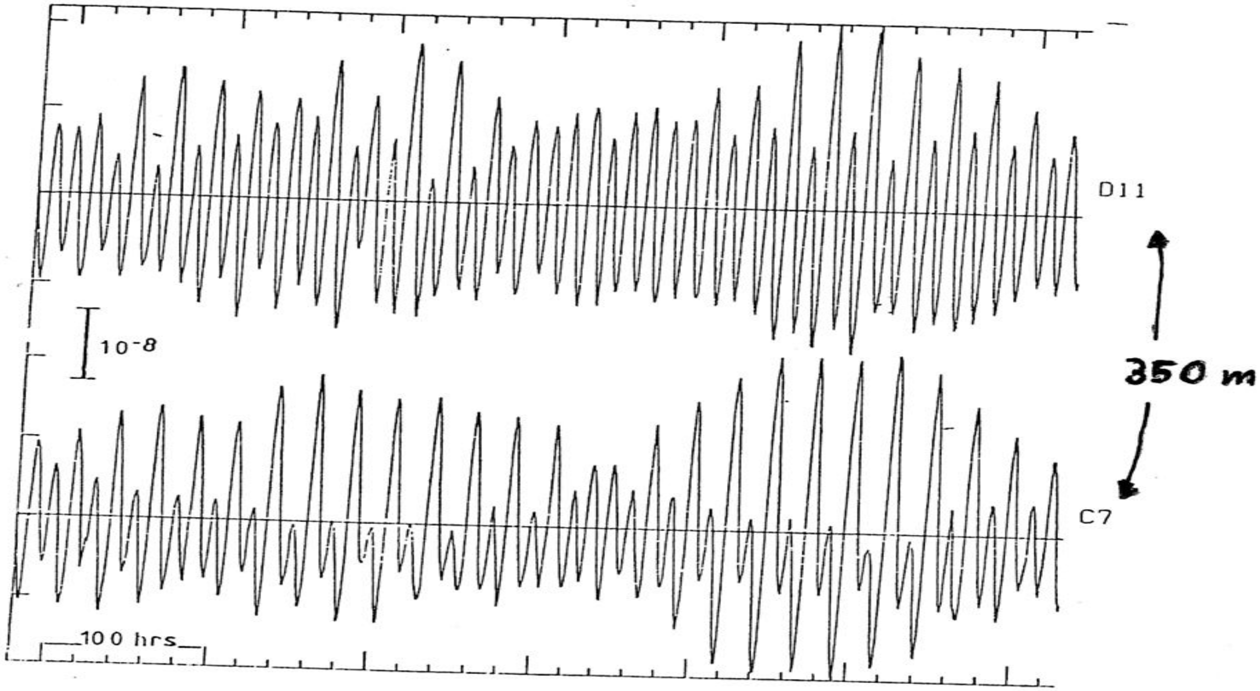

Dissertation David.S. Young, 1980

Figure 1.1 Comparison of tidal strains recorded by two collinear strainmeters. Strain scale is only very approximate.

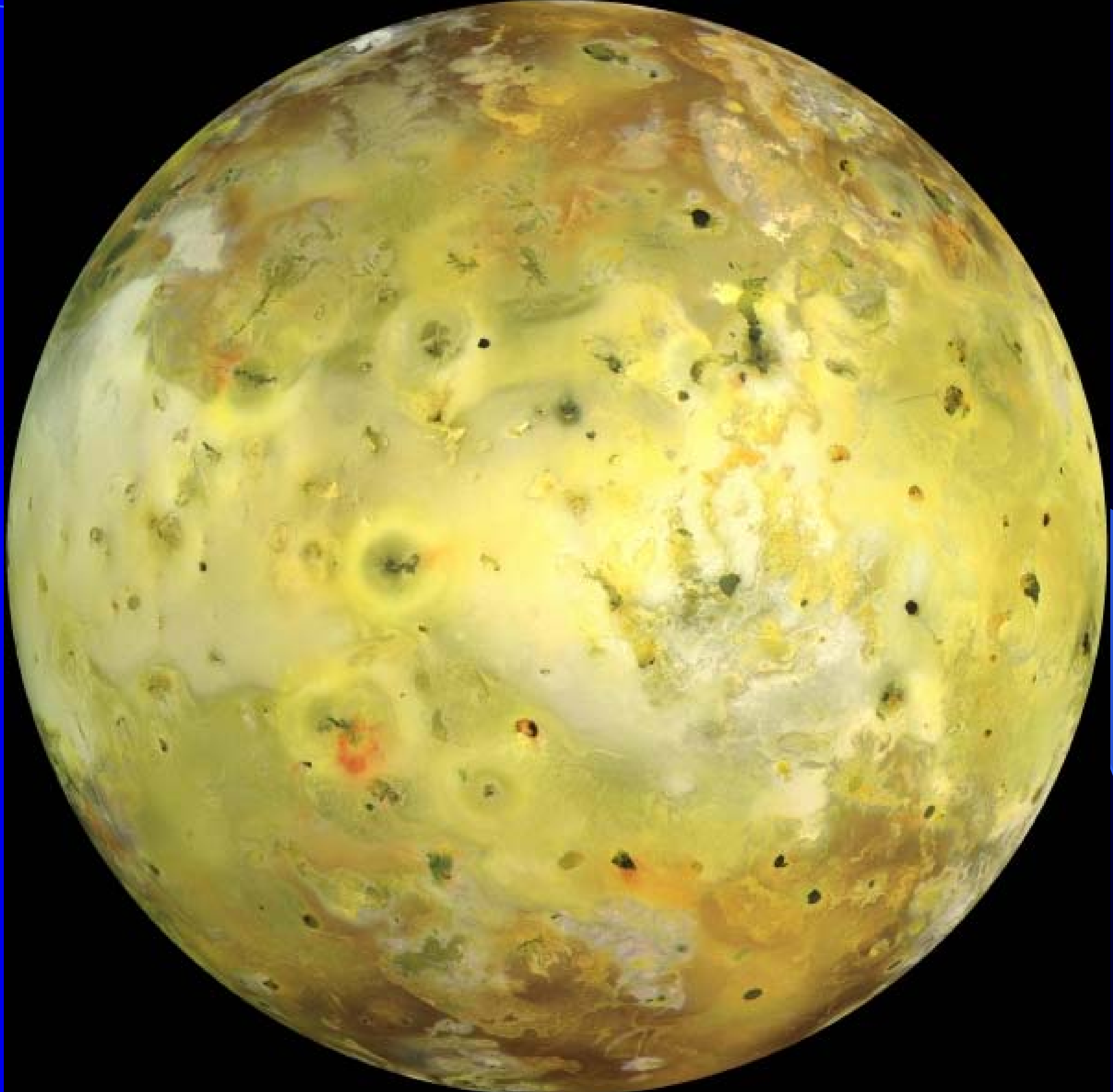

Conversion to geocentric coordinates

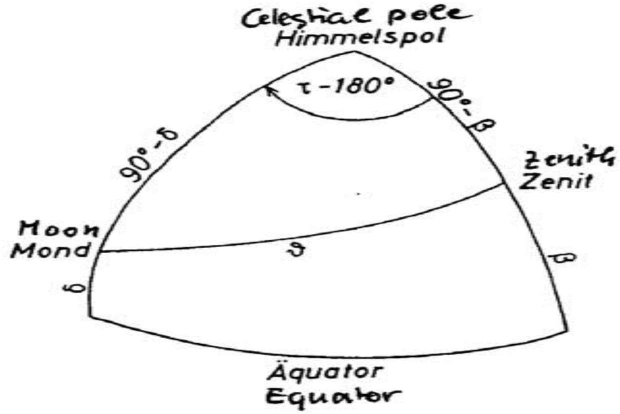

β – geocentric latitude of station

δ – declination of tide-raising body (here: moon)

τ – hour angle of tide-raising body

ϑ – zenith distance of tide-raising body.

$$\cos \vartheta = \sin\delta \cdot \sin\beta + \cos\delta \cdot \cos\beta \cdot \cos(\pi - \tau)$$

$$= \sin\delta \cdot \sin\beta - \cos\delta \cdot \cos\beta \cdot \cos\tau$$

$$Y_T = - G_D \left\{ \cos 2\vartheta + \frac{1}{3} \right\}$$

$$= - G_D \Big\{ \cos^2\delta \cdot \cos^2\beta \cdot \cos 2\tau$$

$$- \sin^2\delta \cdot \sin^2\beta \cdot \cos\tau$$

$$+ 3\left(\sin^2\delta - \frac{1}{3}\right)\left(\sin^2\beta - \frac{1}{3}\right) \Big\}$$